

FracEKF SIQR Model Analysis TURNITIN (Newest)

by MOHAMMAD GHANI

Submission date: 02-Apr-2024 12:15PM (UTC-0700)

Submission ID: 2338148587

File name: FracEKF_SIQR_Model_Analysis.pdf (4.23M)

Word count: 10659

Character count: 46590

A fractional-order CoVid-19 model: dynamical analysis and predictive results using extended Kalman filter

Mohammad Ghani^{1,*} and Dwi Rantini²

³³
^{1,2}*Data Science Technology, Faculty of Advanced Technology and Multidiscipline,
Universitas Airlangga, Surabaya 60115, Indonesia*

³⁷
Abstract: In this paper, we study dynamics of fractional CoVid-19 model for the CoVid-19 outbreak in Semarang, Indonesia. We first provide the diagram of correlations between isolation rate (ϵ) and infection rate (β) on reproduction number (\mathcal{R}_0) and infected number (V). We can see that reproduction number is directly proportional to infection number and is inversely proportional to isolation rate. For the case of infected number, the varying values of isolation rate provide the meaningful results of dynamical system where the effect of physical distancing is not as significant as the effect of isolation rate. As the results obtained, when the isolation rate increases, then infected number decreases, the susceptible number increases, the quarantined number decreases sharper and the recovered number decreases. For the validation of our fractional CoVid-19 model, then we introduce the fractional extended Kalman filter (FracEKF) as the method to predict our model with the report data of CoVid-19. This FracEKF is the modified version of basic extended Kalman filter due to the memory effect of time-fractional. The prediction results provide the meaningful accuracy of $RMSE$, $NRMSE$, and $MAPE$ for each fractional-order. The varying values of isolation rate also provide the same trends in the report data for the infected number that when the isolation rate increases, then the infected number decreases. Moreover, for the varying fractional-order, the higher the fractional-order is, the higher the accuracy is. We further obtain that the higher the varying Q_f is the smaller the error values are (it is closer to the report data for varying fractional-order α) and the higher the varying R_f is the higher the error values are (it gets further away from the report data for varying fractional-order α). The profiles $RMSE$, $NRMSE$ and $MAPE$ are that Q_f is inversely proportional to $RMSE$, $NRMSE$ and $MAPE$, R_f is directly proportional to $RMSE$, $NRMSE$ and $MAPE$ and α is inversely proportional to $RMSE$, $NRMSE$ and $MAPE$.

Keywords: fractional-order model; CoVid-19; transmission rate; fractional extended Kalman filter (FracEKF).

AMS (2020) Subject Classification: 35A01, 35B40.

*Corresponding Author

E-mail address: mohammad.ghani2013@gmail.com

1 Introduction

Since 2019, the Covid-19 outbreak caused by a Coronavirus occurred. The symptoms of Coronaviruses caused fever and shortness of breath. Moreover, the CoVid-19 outbreak in Indonesia was firstly on 2nd March, 2020 [20]. In the middle April 2023, the Ministry of Health reported the newest variant called as Arcturus giving the meaningful impact in Indonesia where this variant was formed by two or more homologous recombination sublineages [33].

The implementation of mathematics is a concern to provide the prediction of outbreak transmission. The simplest *SI* model derived from the Bernoulli Verhulst model can identify the parameters [17]. The next model that considers recovery aspect, the *SIR* model is employed to give the prediction of medical treatment [3]. The model of *SIR* is constructed to decrease the number of outbreak transmission according to room availability [6]. The cleanliness awareness and physical distancing are the aspects which can help to decrease the Covid-19 outbreak transmission[8] and the another study promotes the local restrictions, short-term comparison with Verhulst, Gompertz, and the influence of the health system respectively to this *SIR* model [14, 21, 5]. We notice that the *SIR* model provides the interaction level and intensity of recovery [30], where the nonstandard finite difference method is employed to this *SIR* model [43].

A parameter-varying modification of the *SIRD* model was studied in [11] to capture possible structural changes of the epidemic characteristics and a reliable predictions of the infection evolution of CoVid-19 in the short-term was addressed in [35]. The long-term prediction of *SIRD* model for case in Indonesia are employed to predict the CoVid-19 outbreak [36]. As the results obtained, the infection rate of a younger individuals is more possible than an older individuals [13]. Another study, the *SEIR* model of CoVid-19 outbreak including the exposed sub-individuals provide the impact of control to the hybrid model by considering the vaccination and isolation [28, 7]. The adaptive *SIRV* model employed the inverse problem approach to estimate parameters where the vaccine efficacy can provide the impacts of disease transmission and prevent the transmission at the same rate [34]. The hybrid model of *SVEIR* employed two vaccination doses and delay effects where the time delay indicates the time needed by vaccination to provide immune protection against SARS-CoV-2 [41]. The vaccination campaign was also applied to *SVIR* model by providing the estimation of parameters using ordinary least square [38] and *SIQRD* model for the targeted vaccination allocation increasing the CoVid-19 vaccine benefits amidst its lack of availability [22]. Moreover, the *SIQR* model was addressed in [37] where the effectiveness of different measures was studied for the controlling the outbreak. It has been demonstrated that identifying patients by PCR (Polymerase Chain Reaction) testing and isolating them in a quarantine is more effective than lockdown measures aimed at restricting physical connections in the general community. Moreover, by employing the hybrid model *SIQR*, the environmental noise is an important component in an ecosystem [12]. Therefore, it is vital to disclose how the environmental noise influences the epidemic models. Adnan et al. [1] employed the Atangana-Baleanu-Caputo operator for the *SIQR* model on the spread of Covid-19 which promote the quarantine to decrease the Covid-19 outbreak transmission and the nonstandard finite difference is employed to approximate the numerical results of the hybrid model [2]. Moreover, the other studies of fractional order were studied in [44, 23, 4, 9] where the fractional order can capture not only the current state but also the memory effects and long-rate interactions for the growth rates of system.

Existing CoVid-19 modeling studies, on the other hand, are mostly related to the deterministic models for providing the model profile deterministically through differential equations, where

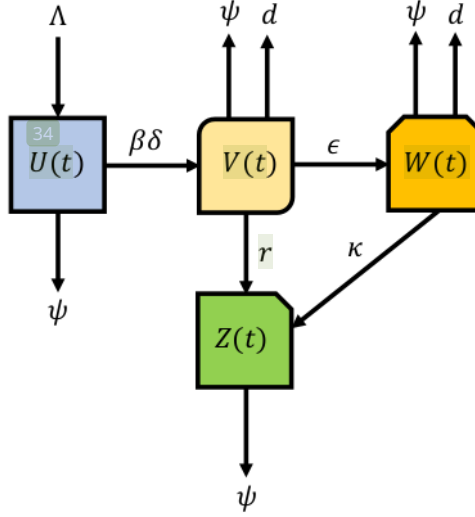


Figure 1: 1st Compartment diagram of CoVid-19 model

this cannot be used to provide the stochastic CoVid-19 model [42, 29]. As a result, in order to obtain the stochastic CoVid-19 model, a stochastic model must be developed. In addition to an epidemiological model, a real-time algorithm for estimating the transmission state online is required for dynamic modeling of the CoVid-19 pandemic. The recursive least squares (RLS) method is a well-known method for estimating model parameters [40, 31]. It can estimate optimal states by determining the minimum linear LS objective function with respect to the system observations. The Kalman filter (KF) presents as an improvement of RLS introducing the states of RLS to obtain a predictive results.

Moreover, the extended Kalman filter (EKF) linearizes the nonlinear dynamical system as an improvement of the KF. EKF provides the simple algorithm and significant computation to solve the nonlinear dynamical system when compared with CLS and MCMC [19, 46]. Hassan et al. introduced the EKF of the SEIR model for CoVid-19 model where the exposed individuals or the incubation period was not considered [25]. To predict CoVid-19 transmission, the EKF of the Lotka-Volterra model was studied in [10] having a limitation of capacity to establish the complex CoVid-19's model for the natural transmission. Meanwhile, the research of CoVid-19 hybrid model estimation for a novel EKF of maximum likelihood refers to [42]. However, this EKF of maximum likelihood arises from deterministic model, then the stochastic CoVid-19 cannot be characterized and also re-infection and physical distancing were ignored.

The proposed model in this paper is based on the study in [15, 16], where the growth rates of those two studies only provide the current state and do not consider the physical distancing (δ) and isolation (ϵ) rates. Then, the Caputo fractional derivative is considered in this paper, where the definition is given below.

Definition 1. (See [39]). Let $\alpha > 0$. Then for function $f \in C^n$, the Caputo fractional derivative

with order α is given by

$$D_*^\alpha f(t) = \frac{1}{\Gamma(n-\alpha)} \int_0^t \frac{f^{(n)}(s)}{(t-s)^{1+\alpha-n}} ds, \quad (1.1)$$

where $n = \lceil \alpha \rceil$.

For the particular case of $0 < \alpha \leq 1$, the equation (1.1) can be derived as follows

$$D_*^\alpha f(t) = \frac{1}{\Gamma(1-\alpha)} \int_0^t \frac{f'(s)}{(t-s)^\alpha} ds. \quad (1.2)$$

Due to the nonlocal operator of Caputo fractional derivative (the initial and current states are considered, [26, 27]), we modify the dynamical system in [15, 16] by employing the Caputo fractional derivative and the aspects of physical distancing (δ) and isolation (ϵ) rates are also considered. Therefore, the first derivatives of dynamical system in [15, 16] are replaced by the Caputo fractional derivative to obtain

$$\begin{aligned} D_*^\alpha U &= \Lambda - \beta \delta UV - \psi U, \\ D_*^\alpha V &= \beta \delta UV - (r + \epsilon + \psi + d)V, \\ D_*^\alpha W &= \epsilon V - (\kappa + d + \psi)W, \\ D_*^\alpha Z &= rV + \kappa W - \psi Z, \end{aligned} \quad (1.3)$$

where $U(0) = U_0, V(0) = V_0, W(0) = W_0, Z(0) = Z_0, 0 < \alpha \leq 1$ and the descriptions of all model parameters are presented in Table 1 and the values as well. The range of values for physical distancing is between zero (the highest level of physical distancing) and one (the lowest level of physical distancing). As shown in Fig. 1, the susceptible individuals (U) goes to the infected individuals (V) if there is a contact with the transmission rate (β). The number of infected individuals will degrade if the physical distancing (δ) increases. The infected individuals (V) goes to two possibilities (the quarantined individuals (W) or the recovered individuals (Z)). The infected individuals goes to the quarantined individuals with the isolation rate (ϵ) if the symptoms increase and require the treatment. Moreover, the infected individuals goes to the recovered individuals with the recovery rate (r) if the symptoms decrease and this can be due to the immune system in the body. The quarantined individuals (W) goes to the recovered individuals (Z) if the symptoms decrease and this can be due to the immune system in the body and also the treatment during the quarantine period. There is a possible number of mortality with the rate (d) due to CoVid-19 during the infection and quarantine period and there is also the natural mortality caused by other than CoVid-19 (ψ). The extended Kalman filter is employed to provide the predictive results with the report data of CoVid-19. Due to the influence of memory effect and long-range interactions in the proposed model, then we need to modify the extended Kalman filter for the fractional stochastic CoVid-19 model. Therefore, we introduce the fractional extended Kalman filter (FracEKF) to overcome this memory effect of our fractional CoVid-19 model.

2 Dynamical analysis

Lemma 1. (See [24]). Suppose that the fractional-order $0 < \alpha \leq 1$ exists and the continuous function $\varphi(t)$ in \mathbb{R}_+ , then one can derive

$$D_*^\alpha \left(\varphi(t) - \varphi^* - \varphi^* \ln \frac{\varphi(t)}{\varphi^*} \right) \leq \left(1 - \frac{\varphi^*}{\varphi(t)} \right) D_*^\alpha \varphi(t), \quad (2.1)$$

where $\varphi^* \in \mathbb{R}_+$ and any $t > 0$.

2.1 Property of boundedness and non-negativity

Theorem 2.1. All variables $(U, V, W, Z)(t) \geq 0$ in a region $\Pi = \left\{ \mathcal{N}(t) \in \mathbb{R}^4 : \mathcal{N}(t) \leq \frac{\Lambda}{\psi} \right\}$ are bounded for all $t > 0$. 31

Proof. Let the total individuals of our CoVid-19 model be defined as $\mathcal{N}(t) = (U + V + W + Z)(t)$ and it satisfies

$$D_*^\alpha \mathcal{N}(t) \leq \Lambda - \psi \mathcal{N}(t).$$

Employing the standard comparison technique (Theorem 1, [24]) provides

$$\mathcal{N}(t) \leq \mathcal{N}(0) \mathcal{M}_\alpha(-\psi t^\alpha) + \frac{\Lambda}{\psi} (1 - \mathcal{M}_\alpha(-\psi t^\alpha)) \quad (\mathcal{M}_\alpha \text{ is Mittage-Leffler function}).$$

As $t \rightarrow +\infty$, one has $\mathcal{M}_\alpha(-\psi t^\alpha) \approx 0$. Consequently, one has

$$\lim_{t \rightarrow +\infty} \sup \mathcal{N}(t) \leq \frac{\Lambda}{\psi}.$$

□

Theorem 2.2. Let $(U, V, W, Z)(0) \geq 0$ be the initial data of dynamical system (1.3). Then, for all $t > 0$, one has $(U, V, W, Z)(t) \geq 0$.

Proof. According to the first equation of (1.3), one has

$$\begin{aligned} D_*^\alpha U(t) &= \Lambda - \beta \delta U V - \psi U \\ &\geq -(\beta \delta V + \psi) U = -\left(\frac{\Lambda \beta \delta}{\psi} + \psi\right) U. \end{aligned}$$

It follows from the standard comparison technique (Theorem 1, [24]), one provides

$$U(t) \geq (U(0) - 0) \mathcal{M}_\alpha\left(-\left(\frac{\Lambda \beta \delta}{\psi} + \psi\right) t^\alpha\right) \quad (\mathcal{M}_\alpha \text{ is Mittage-Leffler function}).$$

Due to $\mathcal{M}_\alpha\left(-\left(\frac{\Lambda \beta \delta}{\psi} + \psi\right) t^\alpha\right) \approx 0$ as $t \rightarrow +\infty$, then $U(t) \geq 0$. Similarly, for Mittage-Leffler functions respectively $\mathcal{M}_\alpha(-(r + \epsilon + \psi + d)t^\alpha)$, $\mathcal{M}_\alpha(-(\kappa + d + \psi)t^\alpha)$ and $\mathcal{M}_\alpha(-\psi t^\alpha)$, one has $(V, W, Z)(t) \geq 0$ as $t \rightarrow +\infty$. □

2.2 Equilibrium point

Theorem 2.3. When $\mathcal{R}_0 < 1$, the disease-free equilibrium point $\mathcal{E}_P^0 = \left(\frac{\Lambda}{\psi}, 0, 0, 0\right)$ is established. When $\mathcal{R}_0 > 1$, one has endemic equilibrium point (\mathcal{E}_P^*) , i.e.,

$$\mathcal{E}_P^* = \left(\frac{r + \epsilon + \psi + d}{\beta \delta}, \frac{\Lambda}{r + \epsilon + \psi + d} - \frac{\psi}{\beta \delta}, \frac{\epsilon}{\kappa + d + \psi} V^*, \frac{r V^*}{\psi} + \frac{\kappa W^*}{\psi} \right)$$

Proof. The proof is obtained by employing the steady state, i.e., $D_*^\alpha U(t) = D_*^\alpha V(t) = D_*^\alpha W(t) = D_*^\alpha Z(t) = 0$ for all $t > 0$ and $V = W = 0$ when it is disease-free and $V \neq 0, W \neq 0$ when it is endemic. \square

The further step is to provide the basic reproduction number (\mathcal{R}_0), where this is one of important thing for the mathematical model in epidemiology. The basic reproduction number consists of two aspects, i.e., the transmission matrix (\mathcal{F}) and the transition matrix (\mathcal{V}) which are given as follows

$$\mathcal{F} = \begin{pmatrix} \beta\delta U & 0 \\ 0 & 0 \end{pmatrix}, \quad \mathcal{V} = \begin{pmatrix} (r + \epsilon + \psi + d) & 0 \\ -\epsilon & \kappa + d + \psi \end{pmatrix}.$$

Based on the existence of equilibrium points at disease-free and the calculation of next generation matrix ($\mathcal{F}\mathcal{V}^{-1}$) as in [18], we consider the following basic reproduction number for our dynamical system

$$\mathcal{R}_0 = \frac{\Lambda\beta\delta}{\psi(r + \epsilon + \psi + d)}. \quad (2.2)$$

2.3 Stability

Theorem 2.4. When $\mathcal{R}_0 < 1$, one has the local asymptotically stability at the disease-free equilibrium point (\mathcal{E}_P^0). When $\mathcal{R}_0 > 1$, one has the local asymptotically stability at the endemic equilibrium point (\mathcal{E}_P^*).

Proof. The proof is obtained by determining the eigenvalue (λ) characteristic, i.e., for disease-free equilibrium point, it is stable when $\lambda < 0$ and it is unstable when $\lambda > 0$ through the following Jacobian matrix

$$J(\mathcal{E}_P^0) = \begin{pmatrix} -\psi & -\frac{\Lambda\beta\delta}{\psi} & 0 & 0 \\ 0 & \frac{\Lambda\beta\delta}{\psi} - (r + \epsilon + \psi + d) & 0 & 0 \\ 0 & \epsilon & -(\kappa + d + \psi) & 0 \\ 0 & r & \kappa & -\psi \end{pmatrix}.$$

By utilizing the formula $\det(J((\mathcal{E}_P^0) - \lambda I)) = 0$ for the Jacobian matrix above, then one has the characteristic equation

$$(-\psi - \lambda)^2(-(\kappa + d + \psi) - \lambda) \left(\frac{\Lambda\beta\delta}{\psi} - (r + \epsilon + \psi + d) - \lambda \right) = 0.$$

Then, we can provide the eigenvalues that $\lambda_1 = \lambda_2 = -\psi < 0$, $\lambda_3 = -(\kappa + d + \psi) < 0$ and $\lambda_4 = (r + \epsilon + \psi + d)(\mathcal{R}_0 - 1) < 0$ if $\mathcal{R}_0 < 1$.

The further step is to determine the local stability for the endemic equilibrium point which is obtained based on the Routh-Hurwitz criterion. Similarly, one has the following Jacobian matrix

$$J(\mathcal{E}_P^*) = \begin{pmatrix} -\beta\delta V^* - \psi & -\beta\delta U^* & 0 & 0 \\ \beta\delta V^* & \beta\delta U^* - (r + \epsilon + \psi + d) & 0 & 0 \\ 0 & \epsilon & -(\kappa + d + \psi) & 0 \\ 0 & r & \kappa & -\psi \end{pmatrix}.$$

The similar ways of using the formula $\det(J(\mathcal{E}_P^*) - \lambda I) = 0$ are applied for the Jacobian matrix above, then one provides the eigenvalues $\lambda_1 = -\psi < 0$, $\lambda_2 = -(\kappa + d + \psi) < 0$, and

$$\begin{aligned}\lambda_3 + \lambda_4 &= \text{Tr}(J(\mathcal{E}_P^*)) = -\frac{\Lambda\beta\delta}{r + \epsilon + \psi + d} < 0, \\ \lambda_3 \cdot \lambda_4 &= \text{Det}(J(\mathcal{E}_P^*)) = \psi(\mathcal{R}_0 - 1)(r + \epsilon + \psi + d) + \frac{\Lambda\beta\delta}{r + \epsilon + \psi + d} > 0.\end{aligned}$$

Moreover, the polynomial $p(\lambda) = \lambda^2 + c_1\lambda + c_2$ satisfies the Routh-Hurwitz criterion, i.e., $c_1 > 0$ and $c_1 \cdot c_2 > 0$ then the proof is completed. \square

Theorem 2.5. When $\mathcal{R}_0 < 1$, one has the global asymptotically stability at the disease-free equilibrium point (\mathcal{E}_P^0) . When $\mathcal{R}_0 > 1$, one has the global asymptotically stability at the endemic equilibrium point (\mathcal{E}_P^*) .

Proof. For disease-free equilibrium point (\mathcal{E}_P^0) , we first provide the Lyapunov function

$$\mathcal{L}_F = \left(U - U^0 - U^0 \ln \frac{U}{U^0} \right) + \frac{(r + \epsilon)V}{r + \epsilon + \psi + d} + \frac{\kappa W}{\kappa + d + \psi} + Z.$$

Employing Lemma 1, one can derive

$$D_*^\alpha \mathcal{L}_F \leq \left(\frac{U - U^0}{U} \right) D_*^\alpha U + \frac{(r + \epsilon)D_*^\alpha V}{r + \epsilon + \psi + d} + \frac{\kappa D_*^\alpha W}{\kappa + d + \psi} + D_*^\alpha Z.$$

According to $\Lambda = \psi U^0$ and $\Lambda = \psi Z^0$, one has

$$\begin{aligned}D_*^\alpha \mathcal{L}_F &\leq \left(\frac{U - U^0}{U} \right) (\psi(U^0 - U) - \beta\delta UV) + \frac{(r + \epsilon)(\beta\delta UV - (r + \epsilon + \psi + d)V)}{r + \epsilon + \psi + d} \\ &\quad + \frac{\kappa(\epsilon V - (\kappa + d + \psi)W)}{\kappa + d + \psi} + (rV + \kappa W - \psi Z).\end{aligned}$$

Employing $U(t) \leq \frac{\Lambda}{\psi}$ and $\beta\delta UV = \Lambda - \psi U$, one has

$$D_*^\alpha \mathcal{L}_F \leq -\psi \frac{(U - U^0)^2}{U} - (1 - \mathcal{R}_0)(r + \epsilon + \psi + d)V - (\kappa + d + \psi)W - \frac{(r + d)\Lambda}{\psi}Z. \quad (2.3)$$

Moreover, the right-hand side in Eq. (2.3) is defined as follows

$$\mathcal{B}(t) = \psi \frac{(U - U^0)^2}{U} + (1 - \mathcal{R}_0)(r + \epsilon + \psi + d)V + (\kappa + d + \psi)W + \frac{(r + d)\Lambda}{\psi}Z.$$

Due to $\mathcal{R}_0 < 1$, the function $\mathcal{B}(t)$ is positive. Then, Eq. (2.3) becomes $D_*^\alpha \mathcal{L}_F(t) \leq -\mathcal{B}(t)$ implying that $\mathcal{L}_F(t) + J^\alpha \mathcal{B}(t) \leq \mathcal{L}_F(0) = C$, where J^α is the operator of integration in fractional-order α . Hence

$$J^\alpha \left(\frac{(U - U^0)^2}{U} \right) \leq C, \quad J^\alpha V \leq C, \quad J^\alpha W \leq C \text{ and } J^\alpha Z \leq C.$$

Using the Barbalat's theorem as in [45] and the uniform continuity in Eq. (2.7), then one has $U \rightarrow U^0$ as $t \rightarrow \infty$, $V \rightarrow 0$ as $t \rightarrow \infty$, $W \rightarrow 0$ as $t \rightarrow \infty$ and $Z \rightarrow 0$ as $t \rightarrow \infty$. Therefore $(U, V, W, Z) \rightarrow \left(\frac{\Lambda}{\psi}, 0, 0, 0 \right)$ as $t \rightarrow \infty$ is the initial data in the bounded region Π .

45
Similarly, the global stability for endemic equilibrium point (\mathcal{E}_P^*) , we provide the following Lyapunov function

$$\mathcal{L}_F = \mathcal{L}_{F_1}(U) + \mathcal{L}_{F_2}(V) + \mathcal{L}_{F_3}(W) + \mathcal{L}_{F_4}(Z),$$

where

$$\begin{aligned}\mathcal{L}_{F_1}(U) &= \left(U - U^* - U^* \ln \frac{U}{U^*} \right), \\ \mathcal{L}_{F_2}(V) &= \left(V - V^* - V^* \ln \frac{V}{V^*} \right), \\ \mathcal{L}_{F_3}(W) &= \left(W - W^* - W^* \ln \frac{W}{W^*} \right), \\ \mathcal{L}_{F_4}(Z) &= \left(Z - Z^* - Z^* \ln \frac{Z}{Z^*} \right).\end{aligned}$$

Due to Lemma 1, one has

$$\begin{aligned}D_*^\alpha \mathcal{L}_F &\leq \left(1 - \frac{U^*}{U} \right) D_*^\alpha + \left(1 - \frac{V^*}{V} \right) D_*^\alpha + \left(1 - \frac{W^*}{W} \right) D_*^\alpha + \left(1 - \frac{Z^*}{Z} \right) D_*^\alpha \\ &\leq \mathcal{P}_1 + \mathcal{P}_2 + \mathcal{P}_3 + \mathcal{P}_4,\end{aligned}$$

where

$$\begin{aligned}\mathcal{P}_1 &= \left(1 - \frac{U^*}{U} \right) (\Lambda - \beta \delta UV - \psi U), \\ \mathcal{P}_2 &= \left(1 - \frac{V^*}{V} \right) (\beta \delta UV - (r + \epsilon + \psi + d)V), \\ \mathcal{P}_3 &= \left(1 - \frac{W^*}{W} \right) (\epsilon V - (\kappa + d + \psi)W), \\ \mathcal{P}_4 &= \left(1 - \frac{Z^*}{Z} \right) (rV + \kappa W - \psi Z).\end{aligned}\tag{2.4}$$

3
By utilizing $U = U - U^*$, $V = V - V^*$, $W = W - W^*$ and $Z = Z - Z^*$ into Eq. (2.4) then one has

$$\begin{aligned}D_*^\alpha \mathcal{L}_F &\leq \left(1 - \frac{U^*}{U} \right) (\Lambda - \beta \delta(U - U^*)(V - V^*) - \psi(U - U^*)) + \\ &\quad \left(1 - \frac{V^*}{V} \right) (\beta \delta(U - U^*)(V - V^*) - (r + \epsilon + \psi + d)(V - V^*)) + \\ &\quad \left(1 - \frac{W^*}{W} \right) (\epsilon(V - V^*) - (\kappa + d + \psi)(W - W^*)) + \\ &\quad \left(1 - \frac{Z^*}{Z} \right) (r(V - V^*) + \kappa(W - W^*) - \psi(Z - Z^*)).\end{aligned}$$

After the simplification of calculation above, one can derive $D_*^\alpha \mathcal{L}_F \leq \mathcal{Q}_1 - \mathcal{Q}_2$, where

$$\begin{aligned} \mathcal{Q}_1 &= \Lambda + \frac{\beta\delta V^*(U - U^*)^2}{U} + \frac{\beta\delta U(V - V^*)^2}{V} + \frac{\epsilon(VW + V^*W^*)}{W} + \\ &\quad \frac{r(VZ + V^*Z^*) + \kappa(WZ + W^*Z^*)}{Z}, \\ \mathcal{Q}_2 &= \frac{\Lambda U^*}{U} + \frac{\beta\delta V(U - U^*)^2}{U} + \frac{\psi(U - U^*)^2}{U} + \frac{\beta\delta U^*(V - V^*)^2}{V} + \\ &\quad \frac{(r + \epsilon + \psi + d)(V - V^*)^2}{V} + \frac{\epsilon(V^*W + VW^*)}{W} + \frac{(\kappa + d + \psi)(W - W^*)^2}{W} + \\ &\quad \frac{r(V^*Z + VZ^*) + \kappa(W^*Z + WZ^*)}{Z} + \frac{\psi(Z - Z^*)^2}{Z}. \end{aligned}$$

Therefore, we can show that $D_*^\alpha \mathcal{L}_F < 0$ if $\mathcal{Q}_1 - \mathcal{Q}_2 < 0$ and $\mathcal{Q}_1 - \mathcal{Q}_2 = 0$ if $U = U^*, V = V^*, W = W^*, Z = Z^*$ implying that $D_*^\alpha \mathcal{L}_F = 0$. Hence $D_*^\alpha \mathcal{L}_F \leq \mathcal{Q}_1 - \mathcal{Q}_2 = -\mathcal{G}(t)$ where $\mathcal{G}(t)$ is positive function. The integration results are then obtained $\mathcal{L}_F(t) + J^\alpha \mathcal{G}(t) \leq \mathcal{L}_F(0) = C$, where J^α is the operator of integration in fractional-order α . Moreover, one can derive

$$\begin{aligned} J^\alpha \left(\frac{(U - U^*)^2}{U} \right) &\leq C, \quad J^\alpha \left(\frac{(V - V^*)^2}{V} \right) \leq C, \quad J^\alpha \left(\frac{(W - W^*)^2}{W} \right) \leq C \\ \text{and } J^\alpha \left(\frac{(Z - Z^*)^2}{Z} \right) &\leq C. \end{aligned}$$

Using the Barbalat's theorem as in [45] and the uniform continuity in Eq. (2.7), then one has $U \rightarrow U_8^*$ as $t \rightarrow \infty$, $V \rightarrow V^*$ as $t \rightarrow \infty$, $W \rightarrow W^*$ as $t \rightarrow \infty$ and $Z \rightarrow Z^*$ as $t \rightarrow \infty$. Therefore $(U, V, W, Z) \rightarrow (U^*, V^*, W^*, Z^*)$ as $t \rightarrow \infty$ is the initial data in the bounded region Π . \square

2.4 Property of existence and uniqueness

Theorem 2.6. There exists $(\kappa_1, \kappa_2)(t) \in L^1(0, T) \times L^w(0, T)$ and $t \in [0, T]$ where $w > 1$ for positive maximum time span T . Then, the function $\mathcal{K} : [0, T] \times \mathbb{R} \rightarrow \mathbb{R}$ meets two following conditions

$$\sup_{u \in \mathbb{R}} |\mathcal{K}(t, u)| \stackrel{40}{\leq} \kappa_1(t), \quad \sup_{u, v \in \mathbb{R}, u \neq v} \left| \frac{\mathcal{K}(t, u) - \mathcal{K}(t, v)}{u - v} \right| \stackrel{70}{\leq} \kappa_2(t).$$

Moreover, for any $p_0 \in \mathbb{R}$ we can express Eq. (1.3) into the following general form

$$\begin{aligned} D_*^\alpha P(t) &= \mathcal{K}(t, P(t)), \\ P(0) &= p_0, \end{aligned} \tag{2.5}$$

for a.e. $t \in [0, T]$ and uniquely continuous $P : [0, T] \rightarrow \mathbb{R}$.

Proof. Employing the Riemann-Liouville fractional integral, then Eq. (2.5) can be written as follows

$$P(t) = p_0 + \frac{1}{\Gamma(\alpha)} \int_0^t (t - \xi)^{(\alpha-1)} \mathcal{K}(\xi, P(\xi)) d\xi, \quad t \in [0, T]. \tag{2.6}$$

According to the Picard's iteration, then Eq. (2.6) becomes

$$P_{n+1}(t) = p_0 + \frac{1}{\Gamma(\alpha)} \int_0^t (t-\xi)^{(\alpha-1)} \mathcal{K}(\xi, P_n(\xi)) d\xi,$$

$$P_0(t) = p_0.$$

Due to the continuity of $P_n : [0, T] \rightarrow \mathbb{R}$ for each n , then one has

$$\begin{aligned} \|P_n - p_0\|_{L^\infty(0,T)} &\leq \frac{1}{\Gamma(\alpha)} \left(\int_0^t (t-\xi)^{\frac{\alpha-1}{1-w}} d\xi \right)^{1-w} \left(\int_0^t t_*^{\frac{1}{w}} d\xi \right)^w \int_0^t \sup_{P_{n-1} \in \mathbb{R}} |\mathcal{K}(\xi, P_n(\xi))| d\xi \\ &\leq \frac{t_*^{\frac{1}{w}} (1-w) T^{\alpha-1}}{(\alpha-w)\Gamma(\alpha)} \int_0^t \kappa_1(\xi) d\xi \leq \frac{t_* (1-w) T^{\alpha-1}}{(\alpha-w)\Gamma(\alpha)} \|\kappa_1\|_{L^1(0,T)}. \end{aligned}$$

$$\|P_{n+1} - P_n\|_{L^\infty(0,T)}$$

$$\begin{aligned} &\leq \frac{1}{\Gamma(\alpha)} \left(\int_0^t (t-\xi)^{\frac{\alpha-1}{1-w}} d\xi \right)^{1-w} \left(\int_0^t t_*^{\frac{1}{w}} d\xi \right)^w \\ &\quad \int_0^t \sup_{(P_n, P_{n-1}) \in \mathbb{R}, P_n \neq P_{n-1}} |\mathcal{K}(\xi, P_n(\tau)) - \mathcal{K}(\xi, P_{n-1}(\xi))| d\xi \\ &\leq \frac{t_*^{\frac{1}{w}} (1-w) T^{\alpha-1}}{(\alpha-w)\Gamma(\alpha)} \sup_{(P_n, P_{n-1}) \in \mathbb{R}, P_n \neq P_{n-1}} \left| \int_0^t (P_n(\xi) - P_{n-1}(\xi)) d\xi \right| \int_0^t \kappa_2(\xi) d\xi \quad (2.7) \\ &\leq \frac{t_*^{\frac{1}{w}} (1-w) T^{\alpha-1}}{(\alpha-w)\Gamma(\alpha)} \sup_{(P_n, P_{n-1}) \in \mathbb{R}, P_n \neq P_{n-1}} \left| \int_0^t (P_n(\xi) - P_{n-1}(\xi)) d\xi \right| \int_0^t (\kappa_2(\xi)^w)^{\frac{1}{w}} (t_*)^{1-\frac{1}{w}} d\xi \\ &\leq \frac{t_*^{\frac{1}{w}} (1-w) T^{\alpha-1} \|\kappa_2\|_{L^p} t_*^{1-\frac{1}{w}}}{(\alpha-w)\Gamma(\alpha)} \sup_{(P_n, P_{n-1}) \in \mathbb{R}, P_n \neq P_{n-1}} \left| \int_0^t (P_n(\xi) - P_{n-1}(\xi)) d\xi \right| \\ &\leq \frac{(1-w) T^{\alpha-1} \|\kappa_2\|_{L^p} t_*}{(\alpha-w)\Gamma(\alpha)} \|P_n - P_{n-1}\|_{L^\infty(0,T)}. \end{aligned}$$

where $t_* \leq T$. By using the similar ways for the norms of $\|P_n - P_{n-1}\|$, $\|P_{n-1} - P_{n-2}\|$ until to $\|P_1 - P_0\|$ in $L^\infty(0, T)$, then one can derive

$$\begin{aligned} &\|P_{n+1} - P_n\|_{L^\infty(0,T)} \\ &\leq \frac{(1-w) T^{\alpha-1} \|\kappa_2\|_{L^p} t_*}{(\alpha-w)\Gamma(\alpha)} \|P_n - P_{n-1}\| \leq \dots \leq \left(\frac{(1-w) T^{\alpha-1} \|\kappa_2\|_{L^p} t_*}{(\alpha-w)\Gamma(\alpha)} \right)^n \|\kappa_1\|_{L^1(0,T)}, \end{aligned}$$

giving the completeness of existence proof. The proof of uniqueness is obtained by assuming $r(t) = (r_1 - r_2)(t)$. Then, one gives

$$\begin{aligned} &\|r\|_{L^\infty(0,T)} \\ &\leq \frac{1}{\Gamma(\alpha)} \left(\int_0^t (t-\xi)^{\frac{\alpha-1}{1-w}} d\xi \right)^{1-w} \left(\int_0^t t_*^{\frac{1}{w}} d\xi \right)^w \int_0^t \sup_{(r_1, r_2) \in \mathbb{R}, r_1 \neq r_2} |r_1(\xi) - r_2(\xi)| d\xi \int_0^t \kappa_2(\xi) d\xi \\ &\leq \frac{t_*^{\frac{1}{w}} (1-w) T^{\alpha-1}}{(\alpha-w)\Gamma(\alpha)} \|r\|_{L^\infty(0,T)} \int_0^t (\kappa_2(\xi)^w)^{\frac{1}{w}} (t_*)^{1-\frac{1}{w}} d\xi \\ &\leq \frac{(1-w) T^{\alpha-1} \|\kappa_2\|_{L^p} t_*}{(\alpha-w)\Gamma(\alpha)} \|r\|_{L^\infty(0,T)}. \end{aligned}$$

Due to $w > 1$ and $0 < \alpha \leq 1$, the right-hand side must be smaller than the left-hand side for maximum time span $T > 0$ which provides the contradiction (the state variables are never negative). Then, the solution is satisfied only if $\|r\|_{L^\infty(0,T)} = 0$ or $r_1 = r_2$ indicating the uniqueness of solution. \square

3 Proposed method

The further study of this section is to provide the predictive results (between our model of (1.3) and report data of CoVid-19) by using the fractional extended Kalman filter (FracEKF) where the whole processes can be seen in Fig. 2. As shown in Fig. 2, the FracEKF has two main parts of predicting and updating steps, where $F(\bar{Y}(\zeta|\zeta))$ is the right-hand side of (1.3), $J(\bar{Y}(\zeta|\zeta))$ is the Jacobian matrix (obtained from the derivative results of each state variable) and two fixed values of noises for process Q_f and observation R_f . It follows from study in [32] for numerical results of time-fractional, then we modify the extended Kalman filter (EKF) by involving the memory effect giving an accurate order of $1 - \alpha$ in time. Therefore, the iterative form is given below

$$\hat{Y}(\zeta + 1) = \hat{Y}(\zeta) - E + \Gamma(1 - \alpha) \times (\Delta t)^\alpha \times F(\hat{Y}(\zeta)) + Q_f(\zeta),$$

where E is the memory effect defined as

$$E = \sum_{\eta=1}^{\zeta} \left[(\eta + 1)^{1-\alpha} - \eta^{1-\alpha} \right] \left[\hat{Y}(\zeta + 1 - \eta) - \hat{Y}(\zeta - \eta) \right].$$

[64]

Moreover, Q_f shows the covariance of process and $F(\hat{Y}(m))$ shows the right-hand side of dynamical system (1.3) where \hat{Y} provides all state variables U, V, W, Z . Applying two equations above into the dynamical system (1.3), then one has

$$\begin{aligned} U^{\zeta+1} &= U^\zeta - E_U + \Gamma(1 - \alpha) \times (\Delta t)^\alpha \times \left(\Lambda - \beta \delta U^\zeta V^\zeta - \psi U^\zeta \right) + Q_{f1}^\zeta, \\ V^{\zeta+1} &= V^\zeta - E_V + \Gamma(1 - \alpha) \times (\Delta t)^\alpha \times \left(\beta \delta U^\zeta V^\zeta - (r + \epsilon + \psi + d) V^\zeta \right) + Q_{f2}^\zeta, \\ W^{\zeta+1} &= W^\zeta - E_W + \Gamma(1 - \alpha) \times (\Delta t)^\alpha \times \left(\epsilon V^\zeta - (\kappa + d + \psi) W^\zeta \right) + Q_{f3}^\zeta, \\ Z^{\zeta+1} &= Z^\zeta - E_Z + \Gamma(1 - \alpha) \times (\Delta t)^\alpha \times \left(r V^\zeta + \kappa W^\zeta - \psi Z^\zeta \right) + Q_{f4}^\zeta. \end{aligned}$$

where

$$\begin{aligned} E_U &= \sum_{\eta=1}^{\zeta} \left[(\eta + 1)^{1-\alpha} - \eta^{1-\alpha} \right] \left[U(\zeta + 1 - \eta) - U(\zeta - \eta) \right], \\ E_V &= \sum_{\eta=1}^{\zeta} \left[(\eta + 1)^{1-\alpha} - \eta^{1-\alpha} \right] \left[V(\zeta + 1 - \eta) - V(\zeta - \eta) \right], \\ E_W &= \sum_{\eta=1}^{\zeta} \left[(\eta + 1)^{1-\alpha} - \eta^{1-\alpha} \right] \left[W(\zeta + 1 - \eta) - W(\zeta - \eta) \right], \\ E_Z &= \sum_{\eta=1}^{\zeta} \left[(\eta + 1)^{1-\alpha} - \eta^{1-\alpha} \right] \left[Z(\zeta + 1 - \eta) - Z(\zeta - \eta) \right]. \end{aligned}$$

Let us define that \hat{Y} are the estimated states. Moreover, at the estimated states \hat{Y} , we can derive the following Jacobian matrix of $F(\hat{Y})$

$$J(\hat{Y}) = \begin{pmatrix} \mathcal{N}_{11}(\hat{Y}) & \mathcal{N}_{12}(\hat{Y}) & \mathcal{N}_{13}(\hat{Y}) & \mathcal{N}_{14}(\hat{Y}) \\ \mathcal{N}_{21}(\hat{Y}) & \mathcal{N}_{22}(\hat{Y}) & \mathcal{N}_{23}(\hat{Y}) & \mathcal{N}_{24}(\hat{Y}) \\ \mathcal{N}_{31}(\hat{Y}) & \mathcal{N}_{32}(\hat{Y}) & \mathcal{N}_{33}(\hat{Y}) & \mathcal{N}_{34}(\hat{Y}) \\ \mathcal{N}_{41}(\hat{Y}) & \mathcal{N}_{42}(\hat{Y}) & \mathcal{N}_{43}(\hat{Y}) & \mathcal{N}_{44}(\hat{Y}) \end{pmatrix},$$

where

$$\begin{aligned} \mathcal{N}_{11} &= 1 + \Gamma(1 - \alpha) \times (\Delta t)^\alpha \times (-\beta \delta \hat{V}^\zeta - \psi), \quad \mathcal{N}_{12} = -\Gamma(1 - \alpha) \times (\Delta t)^\alpha \times \beta \delta \hat{U}^\zeta, \\ \mathcal{N}_{13} &= 0, \quad \mathcal{N}_{14} = 0, \\ \mathcal{N}_{21} &= \Gamma(1 - \alpha) \times (\Delta t)^\alpha \times \beta \delta \hat{V}^\zeta, \quad \mathcal{N}_{22} = 1 + \Gamma(1 - \alpha) \times (\Delta t)^\alpha \times (\beta \delta \hat{U}^\zeta - (r + \epsilon + \psi + d)), \\ \mathcal{N}_{23} &= 0, \quad \mathcal{N}_{24} = 0, \\ \mathcal{N}_{31} &= 0, \quad \mathcal{N}_{32} = \Gamma(1 - \alpha) \times (\Delta t)^\alpha \times \epsilon, \quad \mathcal{N}_{33} = 1 + \nu_3 - \Gamma(1 - \alpha) \times (\Delta t)^\alpha \times (\kappa + d + \psi), \\ \mathcal{N}_{34} &= 0, \\ \mathcal{N}_{41} &= 0, \quad \mathcal{N}_{42} = \Gamma(1 - \alpha) \times (\Delta t)^\alpha \times r, \quad \mathcal{N}_{43} = \Gamma(1 - \alpha) \times (\Delta t)^\alpha \times \kappa, \\ \mathcal{N}_{44} &= 1 + \nu_4 - \Gamma(1 - \alpha) \times (\Delta t)^\alpha \times \psi. \end{aligned}$$

The fixed tuning parameters: the covariance of process, the covariance of observation and the square identity matrix are then chosen, which are defined as follows

$$Q_f = \begin{pmatrix} 10 & 0 & 0 & 0 \\ 0 & 10 & 0 & 0 \\ 0 & 0 & 10 & 0 \\ 0 & 0 & 0 & 5 \end{pmatrix}, \quad R_f = \begin{pmatrix} 100 & 0 & 0 & 0 \\ 0 & 10 & 0 & 0 \\ 0 & 0 & 10 & 0 \\ 0 & 0 & 0 & 1 \end{pmatrix}, \quad C = \begin{pmatrix} 1 & 0 & 0 & 0 \\ 0 & 1 & 0 & 0 \\ 0 & 0 & 1 & 0 \\ 0 & 0 & 0 & 1 \end{pmatrix},$$

and the initial P is given below

$$P = \begin{pmatrix} 1000 & 0 & 0 & 0 \\ 0 & 1000 & 0 & 0 \\ 0 & 0 & 1000 & 0 \\ 0 & 0 & 0 & 1000 \end{pmatrix}.$$

The accuracy of our model can be provided through the standard calculations of the root mean square error (*RMSE*), normalized root mean square error (*NRMSE*) and mean absolute percentage error (*MAPE*) which are stated as follows

$$\begin{aligned} RMSE &= \sqrt{\frac{1}{M} \sum_{k=1}^M (\hat{H}_k - H_k)^2}, \quad NRMSE = \frac{\sqrt{\frac{1}{M} \sum_{k=1}^M (\hat{H}_k - H_k)^2}}{\bar{H}_k}, \\ MAPE &= \frac{1}{M} \sum_{k=1}^M \frac{|\hat{H}_k - H_k|}{H_k} \times 100\%, \end{aligned} \tag{3.1}$$

where \hat{H} and H are the predicted results using fractional extended Kalman filter and report data respectively.

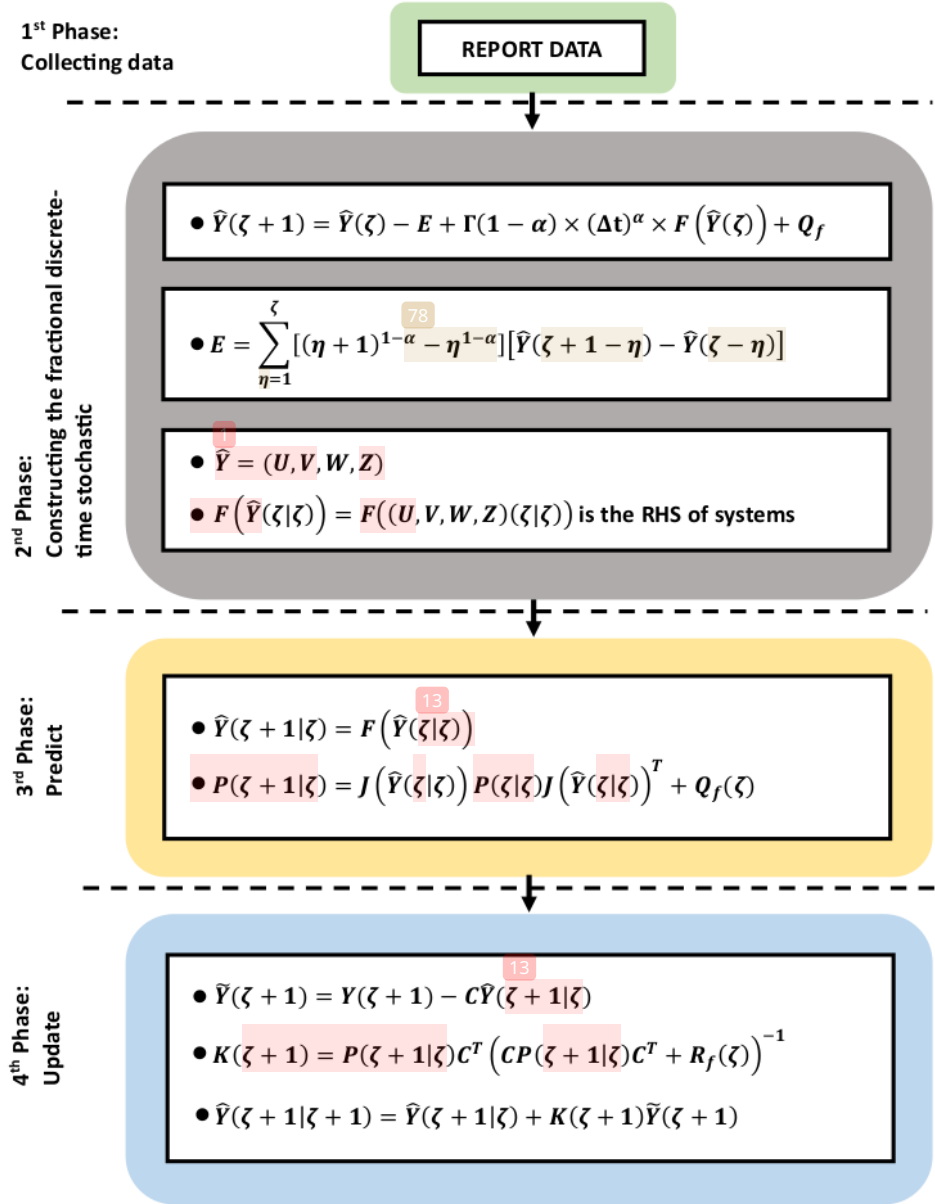


Figure 2: Workflow of fractional extended Kalman filter (FracEKF) based on fractional discrete-time stochastic augmented of CoVid-19 model consisting of state variables (U, V, W, Z) and assumed parameters $(\Lambda, \beta, \delta, \psi, r, \epsilon, d, \kappa)$

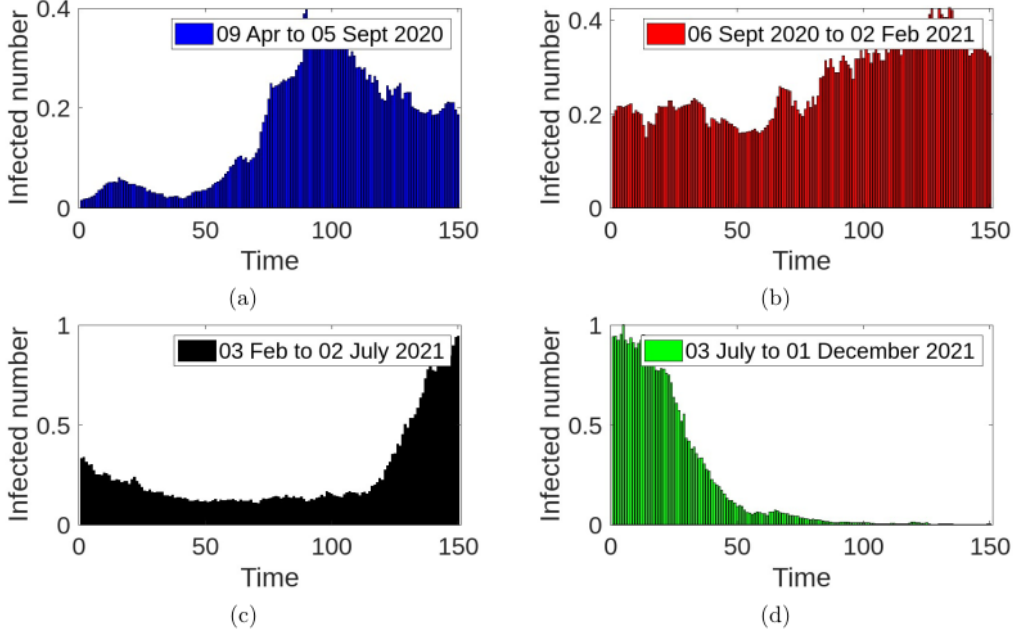


Figure 3: Report data for individuals infected by CoVid-19 and consisting of phase \mathcal{T}_1 (blue color), phase \mathcal{T}_2 (red color), phase \mathcal{T}_3 (black color) and phase \mathcal{T}_4 (green color)

4 Results and discussions

The endemic threshold can be analyzed by the sensitivity index based on the effect of parameters, where all values of sensitivity index are in Table 1 and are visualized in Fig. 5a. Moreover, the sensitivity index can be obtained through the basic reproduction number \mathcal{R}_0 which is differentiable to the parameter π

$$\Gamma_{\pi}^{\mathcal{R}_0} = \frac{\partial \mathcal{R}_0}{\partial \pi} \times \frac{\pi}{\mathcal{R}_0}, \quad (4.1)$$

where

$$\pi = [\Lambda; \beta; \delta; \psi; r; \epsilon; d].$$

The highest sensitivity indices for each model parameter are achieved by the parameters of Λ ($\Gamma_{\Lambda}^{\mathcal{R}_0} = 1$), β ($\Gamma_{\beta}^{\mathcal{R}_0} = 1$) and δ ($\Gamma_{\delta}^{\mathcal{R}_0} = 1$) for the birth rate, transmission and physical distancing rates respectively. This indicates that the birth, transmission and physical distance rates provide the highest impact to increase the individuals infected by CoVid-19, if there are contact directly for two or more individuals. The smallest sensitivity index is only attained by ψ ($\Gamma_{\psi}^{\mathcal{R}_0} = -1$) for the natural mortality rate giving the impact of 100% to degrade the number of individuals infected by CoVid-19. Moreover, the transmission β and physical distancing rates δ give the impact of 100% to increase the number of individuals infected by CoVid-19 because it is directly proportional to the basic reproduction number (\mathcal{R}_0). The similar values of sensitivity

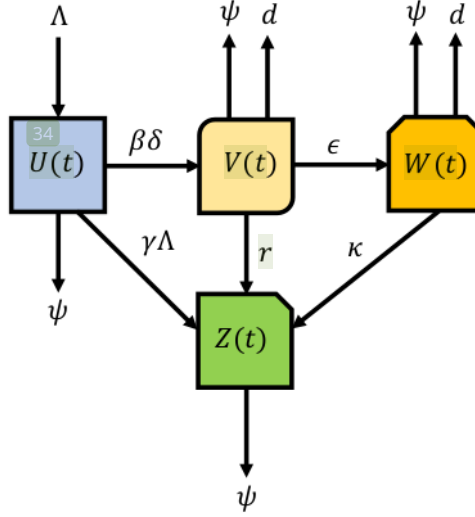


Figure 4: 2nd Compartment diagram of CoVid-19 model

indices (44.10%) are attained by the isolation rate ϵ and recovery rate of infected individuals r , which mean that they have the same impact to degrade the infected number of CoVid-19. According to Eq. (2.2), there is no any effect of κ as the recovery rate of isolated individuals for the change of basic reproduction number. Fig. 5 provides the influence of isolation rate and infection rate on reproduction number and infected number respectively (as in Fig. 5e, the red region provides the higher infected number than the other regions and the red region indicates the highest basic reproduction number ($\mathcal{R}_0 > 1$) as in Fig. 5c). It is clear that the infection rate is directly proportional and is inversely proportional to reproduction number and infected number respectively. The increasing of isolation rate is the most effective way to degrade the transmission of the CoVid-19 outbreak.

As the studies of epidemiology model in [9, 22, 34, 38, 41], the vaccination has the significant impact to decrease the infection rate of disease. Then, we employ the vaccination with rate (γ) for our fractional-order CoVid-19 model as in Fig. 4, where the maximum value of vaccination equals to one and the minimum value of vaccination equals to zero. Table 2 provides the mean values of susceptible (U), infected (V), quarantined (W) and recovered (Z) individuals with and without vaccination. The results indicate that the mean values of susceptible (U), infected (V) and quarantined (W) individuals are decreased after the vaccination but the recovered (Z) individuals is increased after the vaccination. After promoting the vaccination for our fractional-order CoVid-19 model, one has the following basic reproduction number: $\mathcal{R}_0 = \frac{\Lambda(1-\gamma)\beta\delta}{\psi(r+\epsilon+\psi+d)}$, where the basic reproduction number (\mathcal{R}_0) is directly proportional to the vaccination (γ), then we can conclude that the value of basic reproduction number before and after the vaccination can be stated as: $\mathcal{R}_0(\text{with } \gamma) < \mathcal{R}_0(\text{without } \gamma)$, where these results are reasonable with the results in Table 2 that the vaccination can reduce the number of susceptible, infected and quarantined individuals but increase the number of recovered individuals. As the results of prediction for our

Table 1: Model parameter and sensitivity index (SI), where all parameters are assumed and the values of SI are based on the calculations in Eqs. (4.1)-(2.2)

Parameter	Description	Value	SI
Λ	Birth rate	0.07	1
β	Infection rate	0.057	1
δ	Physical distancing rate	0.4	1
ψ	Natural mortality rate	0.0019	-1
r	Recovery rate of infected individuals	0.057	-0.4410
ϵ	Isolation rate	0.03	-0.4410
d	Mortality rate of infected and isolated individuals	0.001	-0.1176
κ	Recovery rate of isolated individuals	0.7	-

fractional-order CoVid-19 model with the report data using FracEKF in Table 3, the vaccination can reduce the mean of infection number for CoVid-19 even though the difference of mean is small between before and after vaccination, namely 0.004, 0.0028 and 0.002 for $\alpha = 0.01$, $\alpha = 0.05$ and $\alpha = 0.09$ respectively. Moreover, the mean values in Fig. 6 are based on the predictive results of infection number for CoVid-19 in Semarang, Indonesia by using FracEKF with eight possibilities (P1, P2, P3, P4, P5, P6, P7 and P8) of physical distancing (δ), isolation rate (ϵ) and vaccination (γ) that are listed as follows: P1 = $[\gamma = 0, \delta = 0, \epsilon = 0]$, P2 = $[\gamma = 0, \delta = 0.4, \epsilon = 0]$, P3 = $[\gamma = 0.5, \delta = 0, \epsilon = 0]$, P4 = $[\gamma = 0, \delta = 0, \epsilon = 0.03]$, P5 = $[\gamma = 0.5, \delta = 0.4, \epsilon = 0]$, P6 = $[\gamma = 0.5, \delta = 0, \epsilon = 0.03]$, P7 = $[\gamma = 0, \delta = 0.4, \epsilon = 0.03]$ and P8 = $[\gamma = 0.5, \delta = 0.4, \epsilon = 0.03]$. According to those eight possibilities, the P6 reaches the smallest infection number caused by CoVid-19 after employing the vaccination ($\gamma = 0.5$) and the isolation ($\epsilon = 0.03$) and the highest infection number is attained by P1 without employing the vaccination ($\gamma = 0$), the isolation ($\epsilon = 0$) and physical distancing ($\delta = 0$). ⁶

The influence of memory effect (the varying fractional-order: $\alpha = 0.75$, $\alpha = 0.8$, $\alpha = 0.85$ and $\alpha = 0.9$) can be shown in Figs. 8a-8d for the endemic ($\mathcal{R}_0 > 1$) and Figs. 7a-7d for disease-free ($\mathcal{R}_0 < 1$). At the disease-free ($\mathcal{R}_0 < 1$), the profiles of infected and quarantined numbers are more sloping than another one ($\mathcal{R}_0 > 1$). The susceptible number of $\mathcal{R}_0 < 1$ is higher than the susceptible number of $\mathcal{R}_0 > 1$ reflecting that the recovered number of $\mathcal{R}_0 < 1$ is lower than the recovered number of $\mathcal{R}_0 > 1$. The quarantined number of $\mathcal{R}_0 < 1$ approaches to zero because this is directly proportional to the infected number of $\mathcal{R}_0 < 1$ which also approaches to zero, i.e., the decreasing of infected number will affect the decreasing of quarantined number in this case. According to the values for all parameters in Table 1, the disease-free ($\mathcal{R}_0 < 1$) is achieved when the physical distancing rate equals to $\delta = 0.04$ and the isolation rate equals to $\epsilon = 0.9$ giving the basic reproduction numbers $\mathcal{R}_0 = 0.9344$ and $\mathcal{R}_0 = 0.8751$ respectively. Based on these results, it indicates that the isolation rate is more effective than the physical distancing to degrade the individuals infected by CoVid-19. If we compare it with the prediction results by using FracEKF as in Fig. 7e, Fig. 8e, Fig. 9e and Fig. 10e, we can conclude that the changes of physical distancing rates (from $\delta = 0.4$ to $\delta = 0.04$) do not provide the significant impact (small difference for increasing of fractional-order α). These results are different from the changes of isolation rate (from $\epsilon = 0.03$ to $\epsilon = 0.9$) giving the significant impact (significant difference for increasing of fractional-order α) as in Figs. 9a-9d and Figs. 10a-10d for all phases (\mathcal{T}_1 , \mathcal{T}_2 , \mathcal{T}_3 , \mathcal{T}_4). Moreover, as the fractional-order increases (from $\alpha = 0.75$ till $\alpha = 0.9$), it needs less time

Table 2: Mean values of susceptible, infected, quarantined and recovered individuals for each fractional-order α with and without vaccination (γ)

Without Vaccination ($\gamma = 0$)											
$\alpha = 0.75$				$\alpha = 0.8$				$\alpha = 0.85$			
U	V	W	Z	U	V	W	Z	U	V	W	Z
2.84	1.23	0.05	5.18	3.01	1.07	0.05	5.78	3.22	0.95	0.04	6.4351
With Vaccination ($\gamma = 0.5$)											
$\alpha = 0.75$				$\alpha = 0.8$				$\alpha = 0.85$			
U	V	W	Z	U	V	W	Z	U	V	W	Z
2.31	1.00	0.04	5.95	2.41	0.82	0.03	6.65	2.59	0.66	0.03	7.38

Table 3: Mean values of report data CoVid-19 for infected individuals (V) using FracEKF for each fractional-order α with and without vaccination (γ)

Without Vaccination ($\gamma = 0$)			With Vaccination ($\gamma = 0.5$)		
$\alpha = 0.01$	$\alpha = 0.05$	$\alpha = 0.09$	$\alpha = 0.01$	$\alpha = 0.05$	$\alpha = 0.09$
0.1420	0.1448	0.1472	0.1380	0.1420	0.1452

to reach the stability for infected and quarantined numbers and it needs more time to reach the stability for susceptible and quarantined numbers (for both $\mathcal{R}_0 < 1$ and $\mathcal{R}_0 > 1$).

The report data of CoVid-19 (from Apr 09 2020 until to Dec 01 2021) is represented in Fig. 3. We further divide it into four phases which are represented as T_1 , T_2 , T_3 and T_4 for Apr 09 to Sept 05 2020 (Fig. 3a), Sept 06 2020 to Feb 02 2021 (Fig. 3b), Feb 03 to July 02 2021 (Fig. 3c) and July 03 to Dec 01 2021 (Fig. 3d) respectively. Fig. 3a reaches the peak point of 0.3967 (976 infected individuals) in 07 July 2020, Fig. 3b reaches the peak point of 0.4260 (1048 infected individuals) in 17 January 2021, Fig. 3c reaches the peak point of 0.9435 (2321 infected individuals) in 02 July 2021 and Fig. 3d reaches the peak point of 1 (2460 infected individuals) in 07 July 2021. The fractional extended Kalman filter (FracEKF) is then employed to our fractional-order model and report data of CoVid-19 and it gives the results significantly showing the good accuracy of $RMSE$, $NRMSE$ and $MAPE$. As in Figs. 9a-9d and Figs. 10a-10d, the infected profiles are still on the pattern even though the varying fractional-order. We can see that the trend of infected number for disease-free case ($\mathcal{R}_0 < 1$ and $\epsilon = 0.9$) is more sloping than the trend of infected number for endemic case ($\mathcal{R}_0 > 1$ and $\epsilon = 0.03$). It follows from those results, we can conclude that the increasing of isolation rate (ϵ) can reduce the infected number significantly. Moreover, Figs. 9a-9d and Figs. 10a-10d also provide the same pattern that the value at peak point increases as the fractional-order α increases (the black line ($\alpha = 0.8$) is the closest distance and the blue line ($\alpha = 0.01$) is the furthest distance with the report data).

Moreover, the values of $RMSE$, $NRMSE$ and $MAPE$ for all phases (T_1 , T_2 , T_3 and T_4) with the varying fractional-order α ($\alpha = 0.01$, $\alpha = 0.05$ and $\alpha = 0.09$) are represented in Fig. 16 and also in Figs. 4-5 for varying Q_f and R_f . We can conclude that the higher the fractional-order is, the better the accuracy is (it is closer between report data and predictive results using FracEKF). As the result of computation time of FracEKF (in unit of seconds) for each phase (T_1 , T_2 , T_3 and T_4) with the varying fractional-order, we symbolize it as ($C_{FracEKF}$). Then, we make

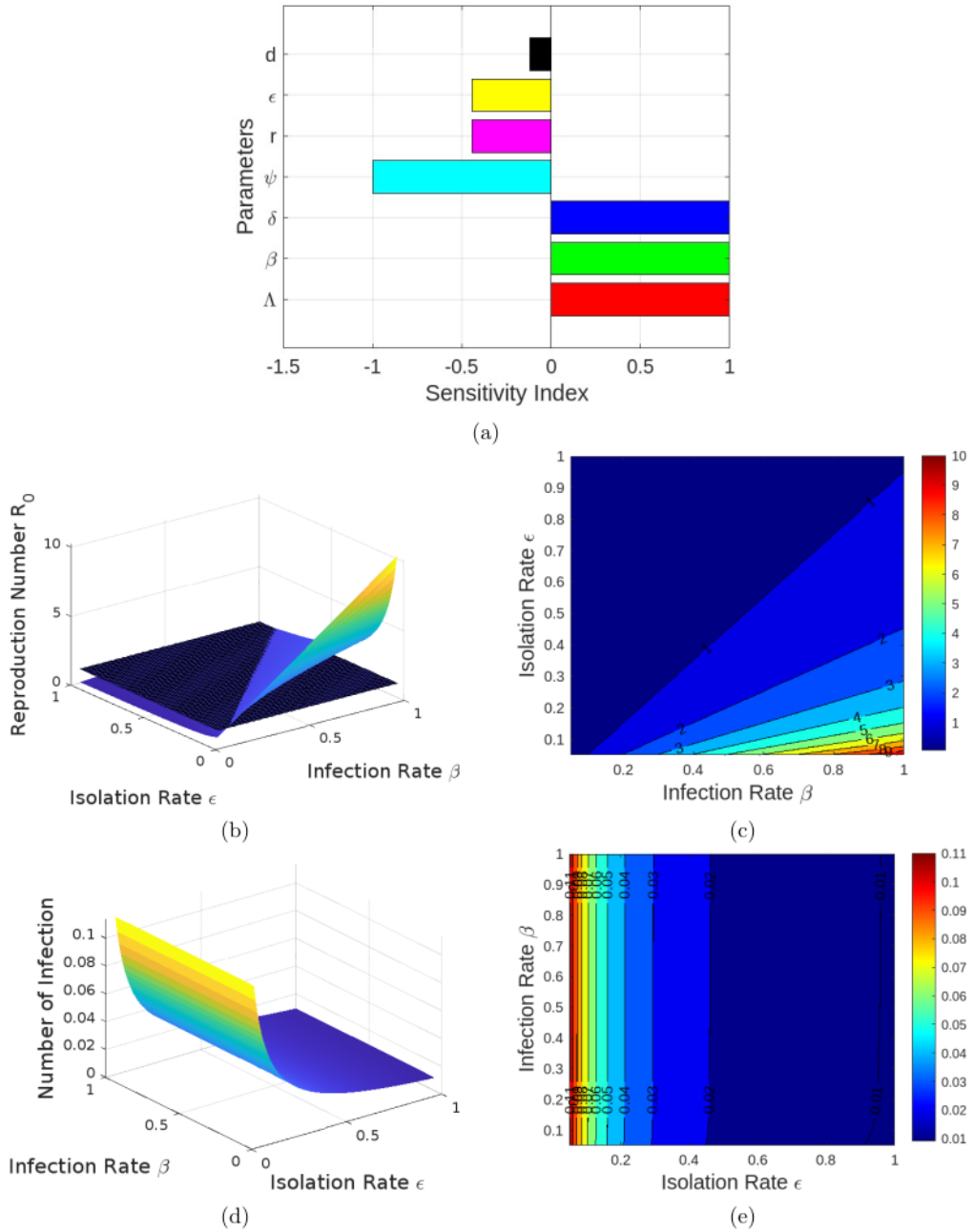


Figure 5: Fig. 5a: Partial Rank Correlation Coefficient, Figs. 5b-5e: Influence of isolation rate and infection rate on reproduction number and on infected number respectively

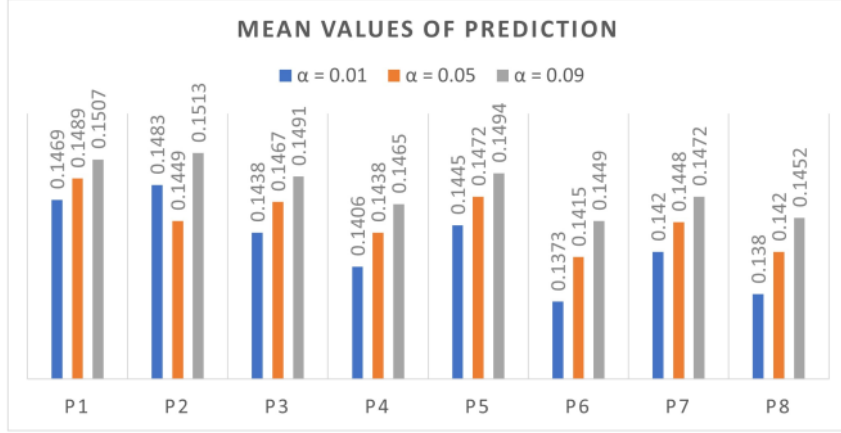


Figure 6: Mean values of individuals infected by CoVid-19 (V) for eight possibilities (P1, P2, P3, P4, P5, P6, P7 and P8) of physical distancing (δ), isolation rate (ϵ) and vaccination (γ)

the list of computation time for each phase as follows: for phase T_1 ($C_{FracEKF}(\alpha = 0.01) = 33.541488$, $C_{FracEKF}(\alpha = 0.05) = 33.565220$ and $C_{FracEKF}(\alpha = 0.09) = 33.820377$), for phase T_2 ($C_{FracEKF}(\alpha = 0.01) = 34.473412$, $C_{FracEKF}(\alpha = 0.05) = 34.255812$ and $C_{FracEKF}(\alpha = 0.09) = 34.166675$), for phase T_3 ($C_{FracEKF}(\alpha = 0.01) = 34.521463$, $C_{FracEKF}(\alpha = 0.05) = 34.375349$ and $C_{FracEKF}(\alpha = 0.09) = 33.932779$) and for phase T_4 ($C_{FracEKF}(\alpha = 0.01) = 34.420729$, $C_{FracEKF}(\alpha = 0.05) = 33.531188$ and $C_{FracEKF}(\alpha = 0.09) = 34.000153$). Meanwhile, the accuracy values for varying Q_f are given in Table 4 and the related error values as in Figs. 11-12. Then, we obtain that the higher the varying Q_f is the smaller the error values are (it is closer to the report data for varying fractional-order α) and the higher the varying R_f is the higher the error values are (it gets further away from the report data for varying fractional-order α) as in Figs. 13-14 where more detailed accuracy values are in Table 5. According to the profiles of RMSE, NRMSE and MAPE as in Fig. 15, the values of RMSE, NRMSE and MAPE increase when R_{f1} , R_{f2} and R_{f3} increase and the values of RMSE, NRMSE and MAPE decrease when Q_{f1} , Q_{f2} and Q_{f3} increase. The values of RMSE, NRMSE and MAPE decrease when α_1 , α_2 and α_3 increase as in Fig. 16. Mathematically, it can be expressed as follows: $(Q_{f1}, Q_{f2}, Q_{f3}) \sim \left(\frac{1}{RMSE}, \frac{1}{NRMSE}, \frac{1}{MAPE} \right)$, $(R_{f1}, R_{f2}, R_{f3}) \sim (RMSE, NRMSE, MAPE)$ and $(\alpha_1, \alpha_2, \alpha_3) \sim \left(\frac{1}{RMSE}, \frac{1}{NRMSE}, \frac{1}{MAPE} \right)$, where Q_f is inversely proportional to RMSE, NRMSE and MAPE, R_f is directly proportional to RMSE, NRMSE and MAPE and α is inversely proportional to RMSE, NRMSE and MAPE.

5 Conclusions

The fractional-order of CoVid-19 model is our concern of this paper. As the results obtained, the reproduction number is directly proportional to infection number and is inversely proportional to isolation rate. This also occurs to case of infected number. The varying values of isolation rate provide the meaningful results for the profiles of our CoVid-19 model for each unit of time, although the effect of physical distancing is not as significant as the effect of isolation

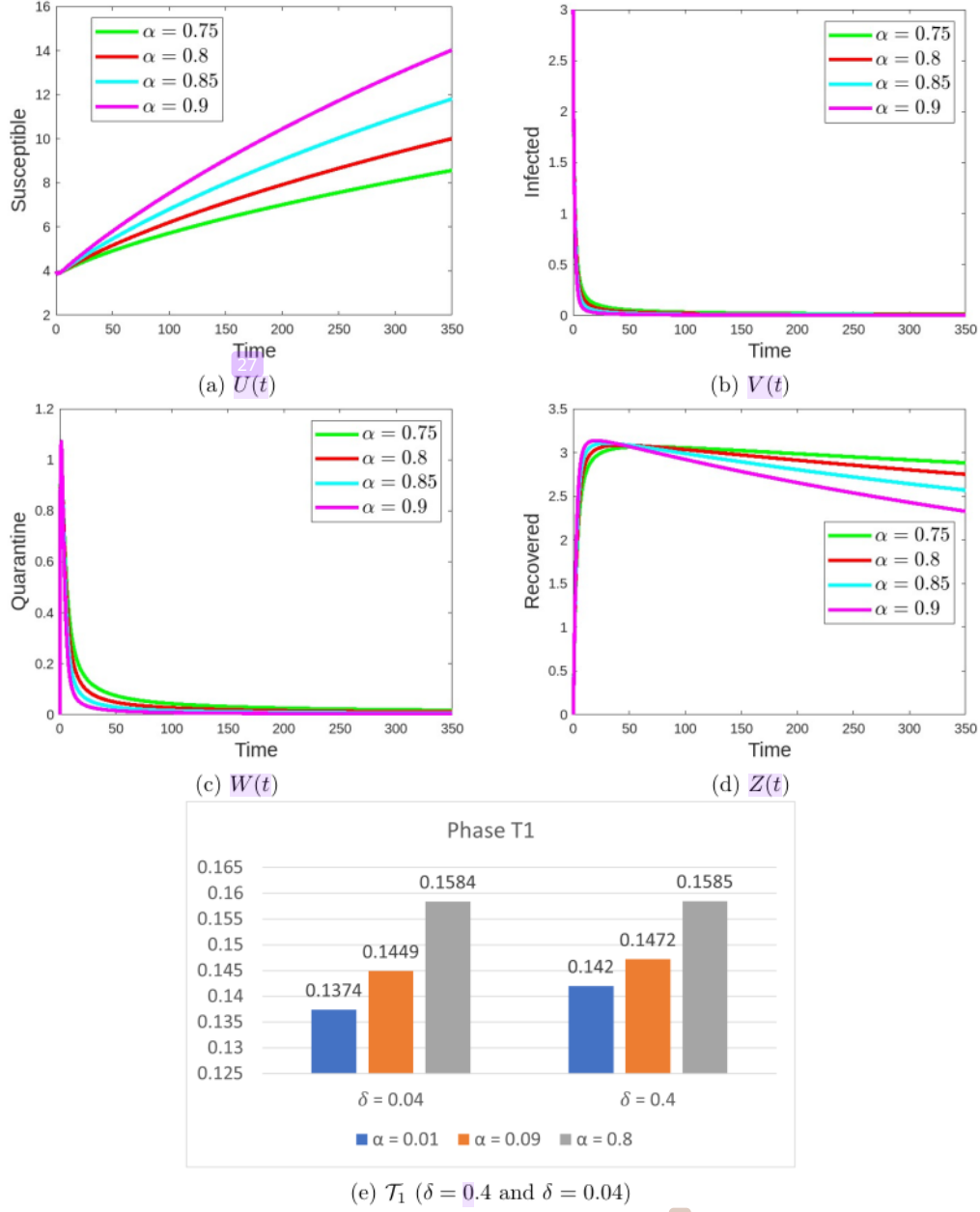


Figure 7: (7a)-(7d): Dynamics of fractional CoVid-19 model for the basic reproduction number $\mathcal{R}_0 < 1$ and (7e): mean values of infected report data with physical distancing $\delta = 0.4$ ($\mathcal{R}_0 > 1$) and $\delta = 0.04$ ($\mathcal{R}_0 < 1$) for phase \mathcal{T}_1

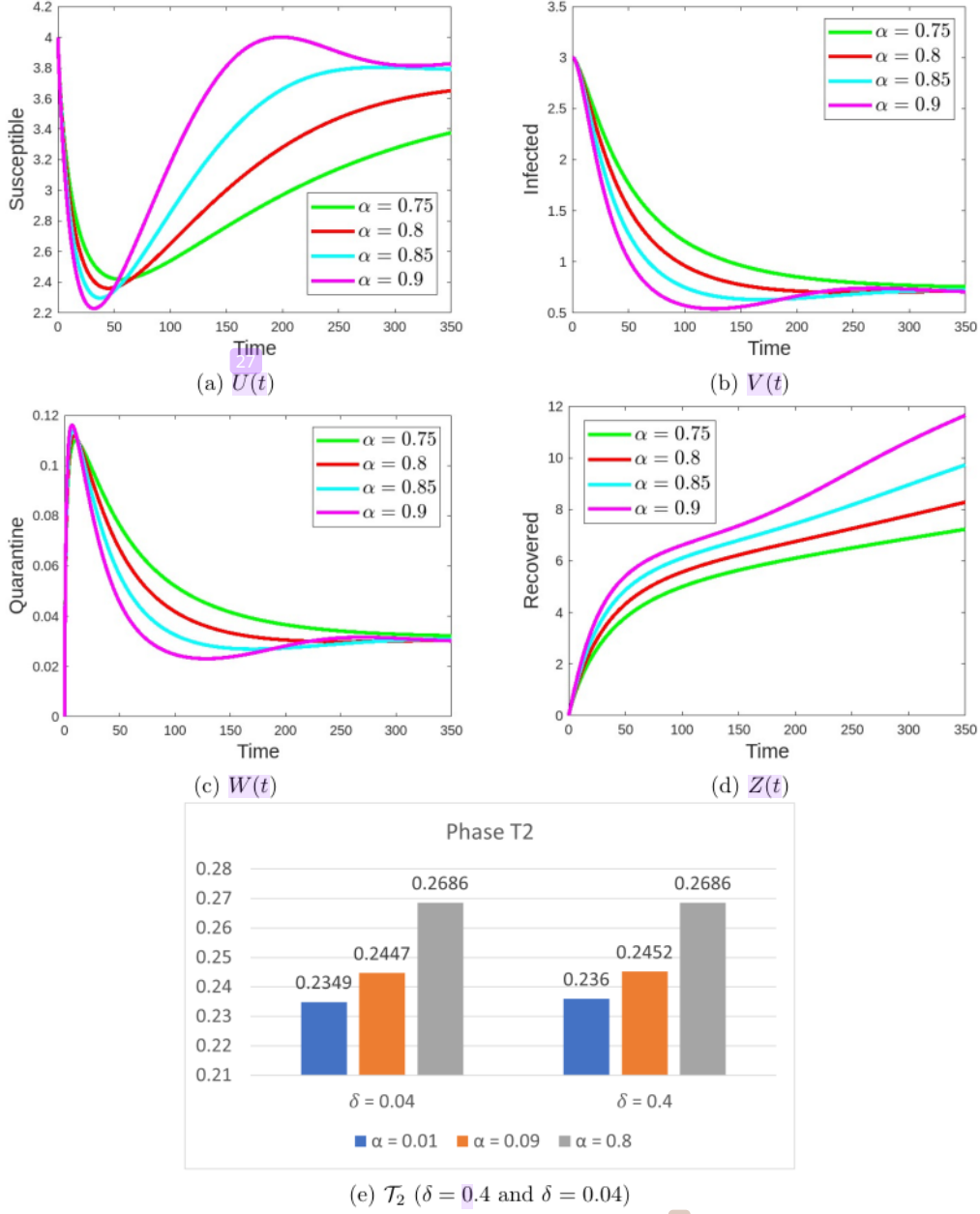


Figure 8: (8a)-(8d): Dynamics of fractional CoVid-19 model for the basic reproduction number $\mathcal{R}_0 > 1$ and (8e): mean values of infected report data with physical distancing $\delta = 0.4$ ($\mathcal{R}_0 > 1$) and $\delta = 0.04$ ($\mathcal{R}_0 < 1$) for phase \mathcal{T}_2

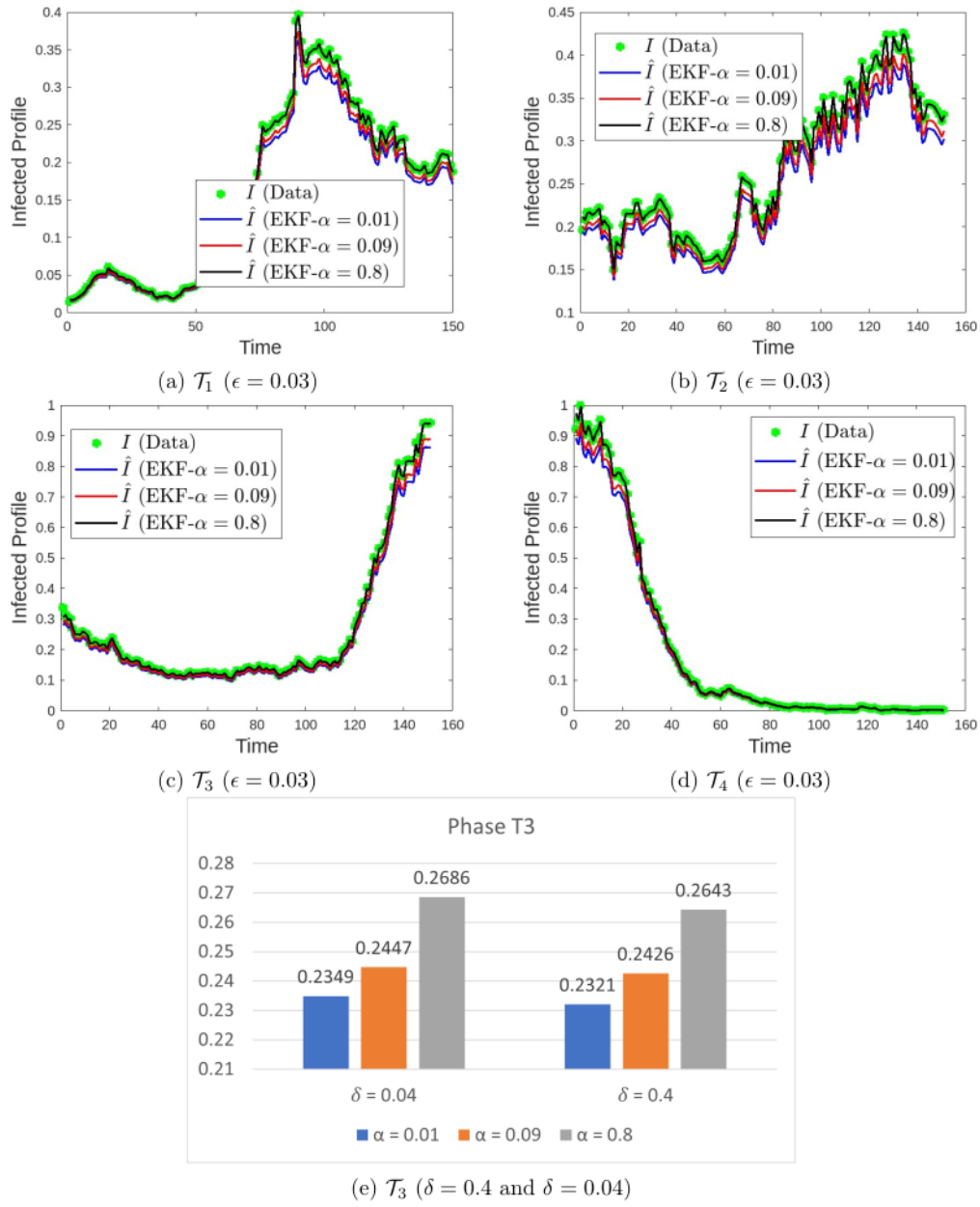


Figure 9: Prediction results of our fractional CoVid-19 model using fractional extended Kalman filter (FracEKF) for (9a)-(9d): the isolation rate $\epsilon = 0.03$ ($\mathcal{R}_0 > 1$) and (9e): mean values of infected report data with physical distancing $\delta = 0.4$ ($\mathcal{R}_0 > 1$) and $\delta = 0.04$ ($\mathcal{R}_0 < 1$) for phase \mathcal{T}_3

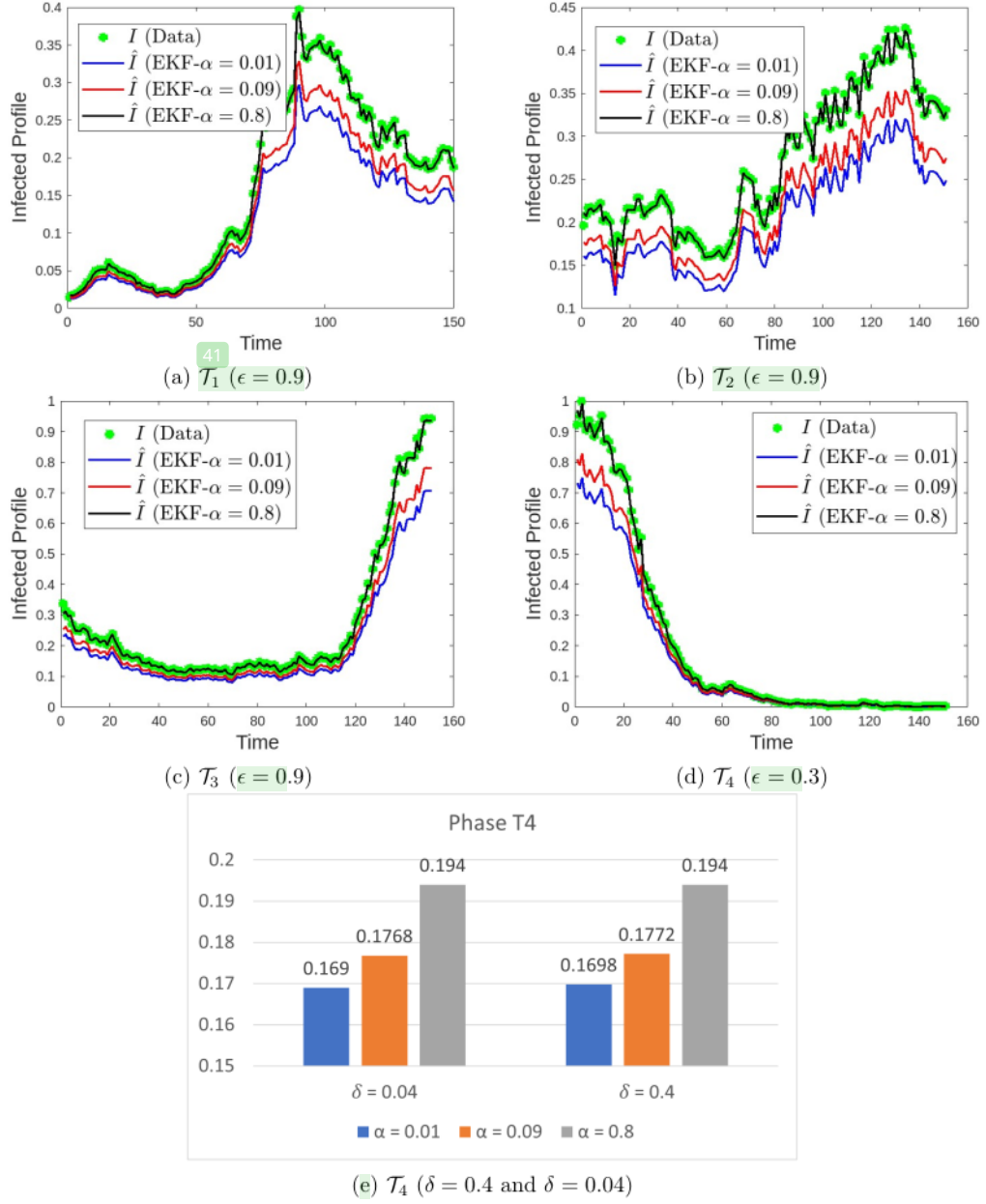


Figure 10: Prediction results of our fractional CoVid-19 model using fractional extended Kalman filter (FracEKF) for (10a)-(10d): the isolation rate $\epsilon = 0.9$ ($\mathcal{R}_0 < 1$) and (10e): mean values of infected report data with physical distancing $\delta = 0.4$ ($\mathcal{R}_0 > 1$) and $\delta = 0.04$ ($\mathcal{R}_0 < 1$) for phase \mathcal{T}_4

Table 4: Accuracy values for (varying Q_f) and (fixed R_f)

phase \mathcal{T}_1					
Varying Q_f and Fixed R_f	Accuracy	$\alpha = 0.01$	$\alpha = 0.05$	$\alpha = 0.09$	
Q_{f1} (Normal)	<i>RMSE</i>	0.0167	0.0136	0.0111	
	<i>NRMSE</i>	0.1051	0.0858	0.0701	
	<i>MAPE</i>	8.53%	6.99%	5.74%	
Q_{f2} (2 Times)	<i>RMSE</i>	0.0098	0.0080	0.0066	
	<i>NRMSE</i>	0.0620	0.0506	0.0413	
	<i>MAPE</i>	5.09%	4.18%	3.44%	
Q_{f3} (3 Times)	<i>RMSE</i>	0.0071	0.0058	0.0047	
	<i>NRMSE</i>	0.0445	0.0363	0.0297	
	<i>MAPE</i>	3.69%	3.04%	2.52%	
phase \mathcal{T}_2					
Q_{f1} (Normal)	<i>RMSE</i>	0.0238	0.0194	0.0159	
	<i>NRMSE</i>	0.0883	0.0721	0.0589	
	<i>MAPE</i>	8.41%	6.87%	5.62%	
Q_{f2} (2 Times)	<i>RMSE</i>	0.0140	0.0115	0.0094	
	<i>NRMSE</i>	0.0521	0.0426	0.0349	
	<i>MAPE</i>	4.98%	4.07%	3.34%	
Q_{f3} (3 Times)	<i>RMSE</i>	0.0101	0.0083	0.0068	
	<i>NRMSE</i>	0.0375	0.0307	0.0252	
	<i>MAPE</i>	3.59%	2.94%	2.41%	
phase \mathcal{T}_3					
Q_{f1} (Normal)	<i>RMSE</i>	0.0301	0.0246	0.0202	
	<i>NRMSE</i>	0.1133	0.0928	0.0762	
	<i>MAPE</i>	8.54%	6.98%	5.72%	
Q_{f2} (2 Times)	<i>RMSE</i>	0.0179	0.0148	0.0122	
	<i>NRMSE</i>	0.0676	0.0556	0.0459	
	<i>MAPE</i>	5.06%	4.14%	3.40%	
Q_{f3} (3 Times)	<i>RMSE</i>	0.0131	0.0108	0.0090	
	<i>NRMSE</i>	0.0492	0.0407	0.0339	
	<i>MAPE</i>	3.65%	2.99%	2.46%	
phase \mathcal{T}_4					
Q_{f1} (Normal)	<i>RMSE</i>	0.0301	0.0245	0.0199	
	<i>NRMSE</i>	0.1549	0.1261	0.1027	
	<i>MAPE</i>	8.25%	6.73%	5.48%	
Q_{f2} (2 Times)	<i>RMSE</i>	0.0176	0.0144	0.0118	
	<i>NRMSE</i>	0.0909	0.0743	0.0610	
	<i>MAPE</i>	4.85%	3.95%	3.23%	
Q_{f3} (3 Times)	<i>RMSE</i>	0.0127	0.0105	0.0087	
	<i>NRMSE</i>	0.0656	0.0541	0.0450	
	<i>MAPE</i>	3.48%	2.84%	2.31%	

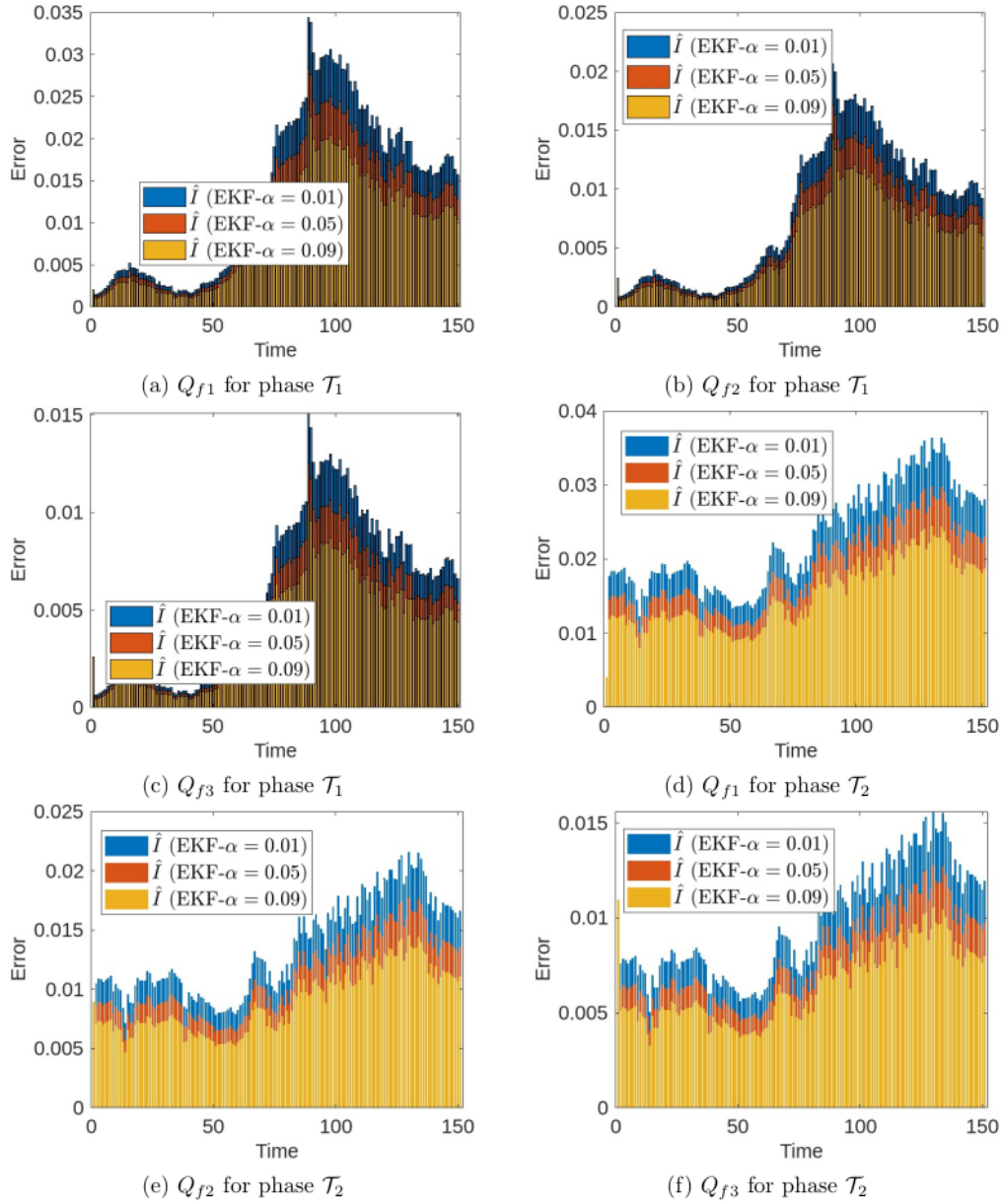


Figure 11: Error values between prediction and report data for varying Q_f : $Q_{f1} = (10; 10; 10; 5)$, $Q_{f2} = (20; 20; 20; 10)$ and $Q_{f3} = (30; 30; 30; 15)$ and phases $(\mathcal{T}_1, \mathcal{T}_2)$

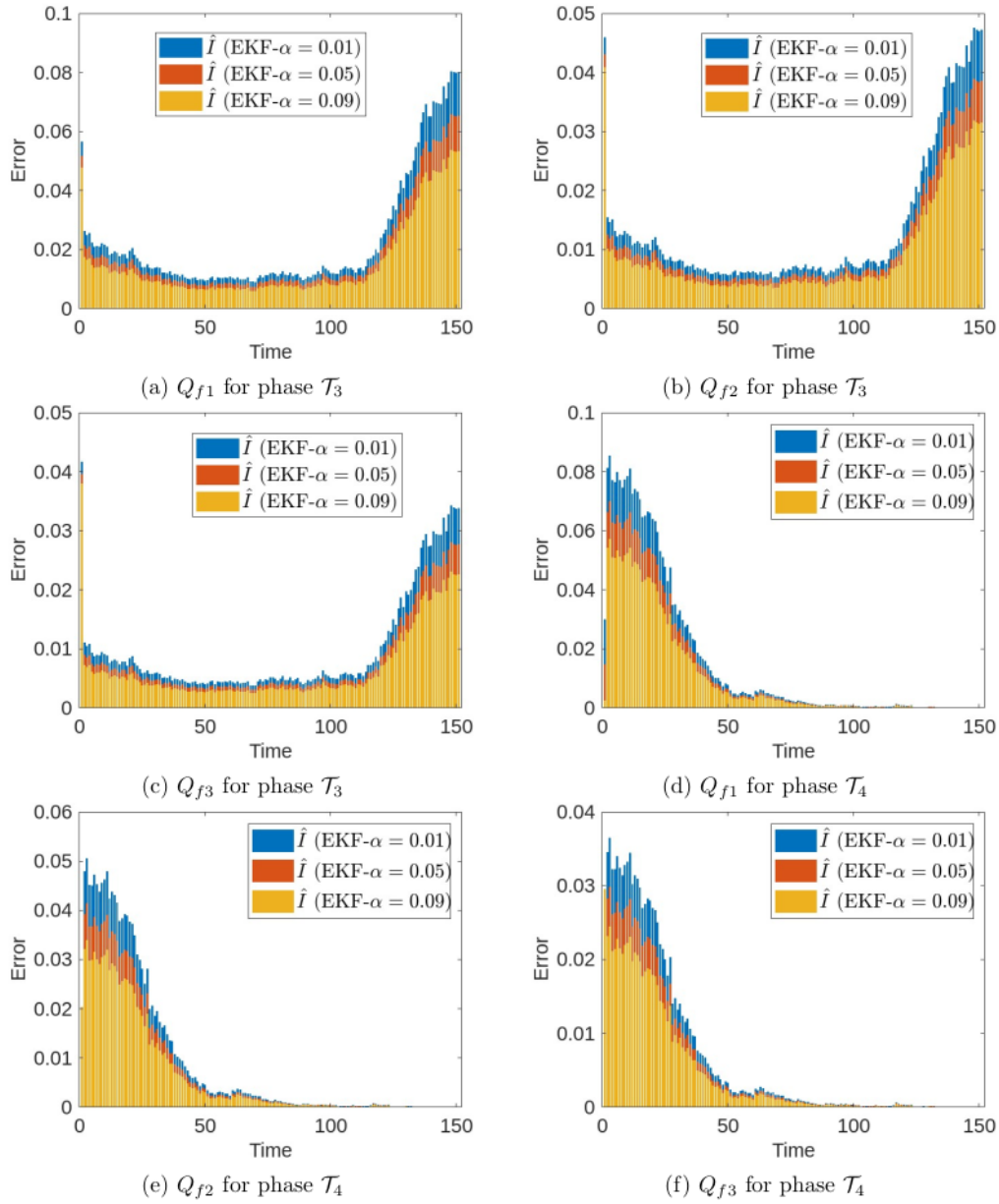


Figure 12: Error values between prediction and report data for varying Q_f : $Q_{f1} = (10; 10; 10; 5)$, $Q_{f2} = (20; 20; 20; 10)$ and $Q_{f3} = (30; 30; 30; 15)$ and phases $(\mathcal{T}_3, \mathcal{T}_4)$

Table 5: Accuracy values for (varying R_f) and (fixed Q_f)

phase \mathcal{T}_1				
Varying R_f and Fixed Q_f	Accuracy	$\alpha = 0.01$	$\alpha = 0.05$	$\alpha = 0.09$
R_{f1} (Normal)	<i>RMSE</i>	0.0167	0.0136	0.0111
	<i>NRMSE</i>	0.1051	0.0858	0.0701
	<i>MAPE</i>	8.53%	6.99%	5.74%
R_{f2} (2 Times)	<i>RMSE</i>	0.0270	0.0221	0.0180
	<i>NRMSE</i>	0.1700	0.1389	0.1136
	<i>MAPE</i>	13.70%	11.23%	9.21%
R_{f3} (3 Times)	<i>RMSE</i>	0.0350	0.0287	0.0235
	<i>NRMSE</i>	0.2204	0.1806	0.1478
	<i>MAPE</i>	17.73%	14.55%	11.94%
phase \mathcal{T}_2				
R_{f1} (Normal)	<i>RMSE</i>	0.0238	0.0194	0.0159
	<i>NRMSE</i>	0.0883	0.0721	0.0589
	<i>MAPE</i>	8.41%	6.87%	5.62%
R_{f2} (2 Times)	<i>RMSE</i>	0.0384	0.0314	0.0257
	<i>NRMSE</i>	0.1426	0.1166	0.0954
	<i>MAPE</i>	13.62%	11.14%	9.10%
R_{f3} (3 Times)	<i>RMSE</i>	0.0498	0.0408	0.0334
	<i>NRMSE</i>	0.1848	0.1515	0.1242
	<i>MAPE</i>	17.66%	14.48%	11.86%
phase \mathcal{T}_3				
R_{f1} (Normal)	<i>RMSE</i>	0.0301	0.0246	0.0202
	<i>NRMSE</i>	0.1133	0.0928	0.0762
	<i>MAPE</i>	8.54%	6.98%	5.72%
R_{f2} (2 Times)	<i>RMSE</i>	0.0483	0.0396	0.0325
	<i>NRMSE</i>	0.1822	0.1492	0.1223
	<i>MAPE</i>	13.77%	11.27%	9.23%
R_{f3} (3 Times)	<i>RMSE</i>	0.0625	0.0513	0.0421
	<i>NRMSE</i>	0.2357	0.1935	0.1587
	<i>MAPE</i>	17.83%	14.63%	11.99%
phase \mathcal{T}_4				
R_{f1} (Normal)	<i>RMSE</i>	0.0301	0.0245	0.0199
	<i>NRMSE</i>	0.1549	0.1261	0.1027
	<i>MAPE</i>	8.25%	6.73%	5.48%
R_{f2} (2 Times)	<i>RMSE</i>	0.0489	0.0399	0.0325
	<i>NRMSE</i>	0.2520	0.2055	0.1675
	<i>MAPE</i>	13.34%	10.91%	8.91%
R_{f3} (3 Times)	<i>RMSE</i>	0.0636	0.0520	0.0425
	<i>NRMSE</i>	0.3276	0.2679	0.2188
	<i>MAPE</i>	17.25%	14.16%	11.60%

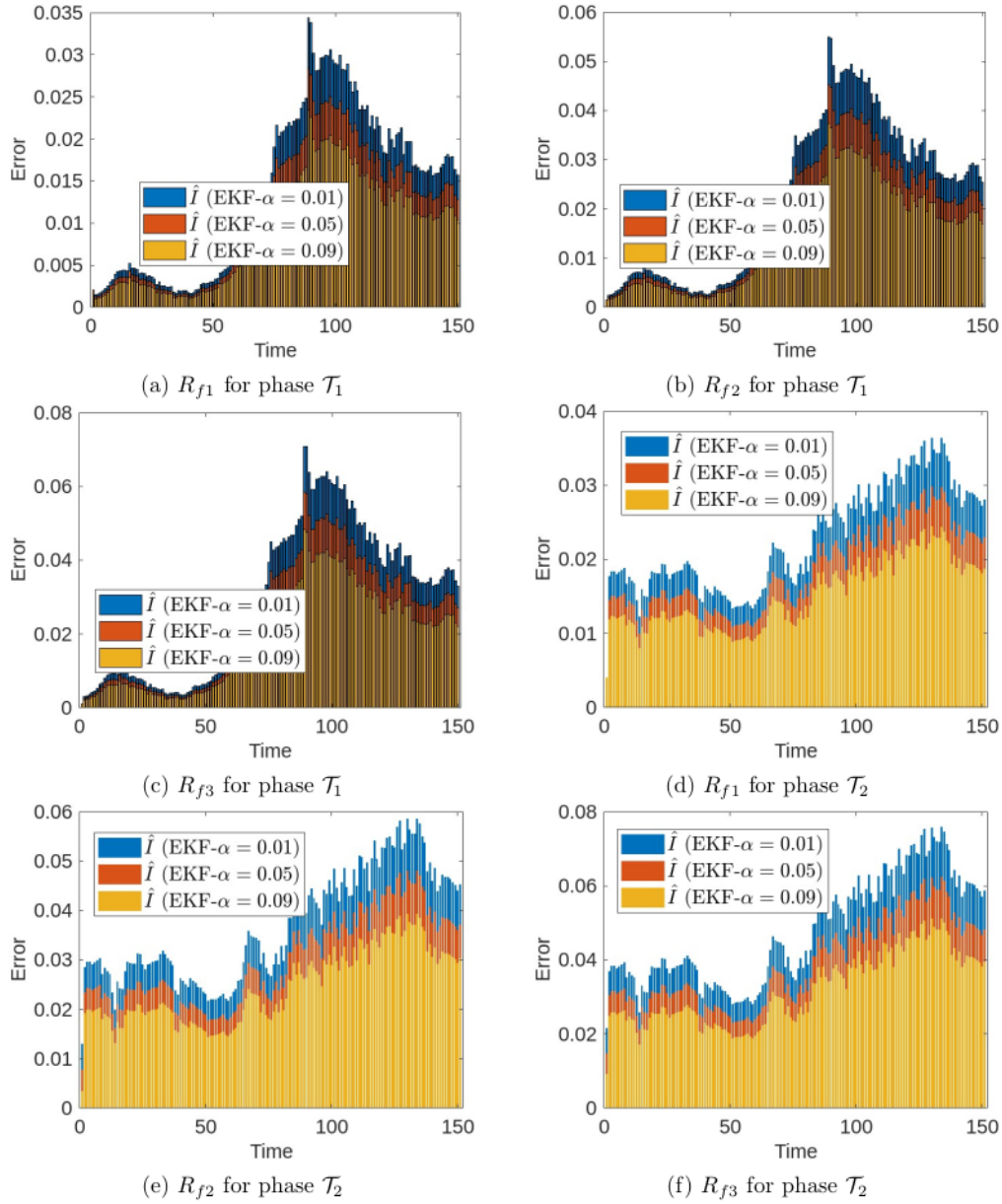


Figure 13: Error values between prediction and report data for varying R_f : $R_{f1} = (100; 10; 10; 1)$, $R_{f2} = (200; 20; 20; 2)$ and $R_{f3} = (300; 30; 30; 3)$ and phases $(\mathcal{T}_1, \mathcal{T}_2)$

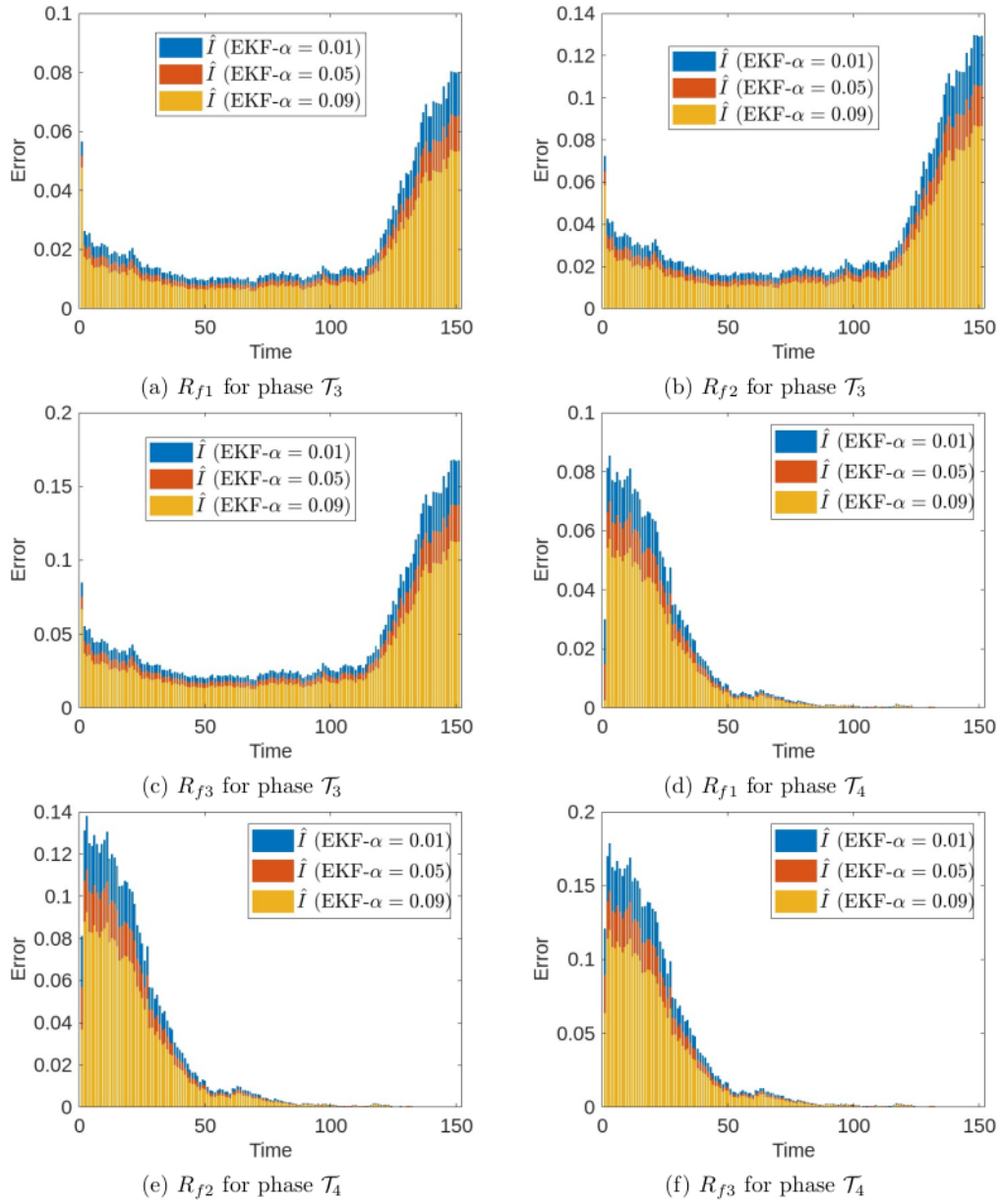


Figure 14: Error values between prediction and report data for varying R_f : $R_{f1} = (100; 10; 10; 1)$, $R_{f2} = (200; 20; 20; 2)$ and $R_{f3} = (300; 30; 30; 3)$ and phases (T_3, T_4)

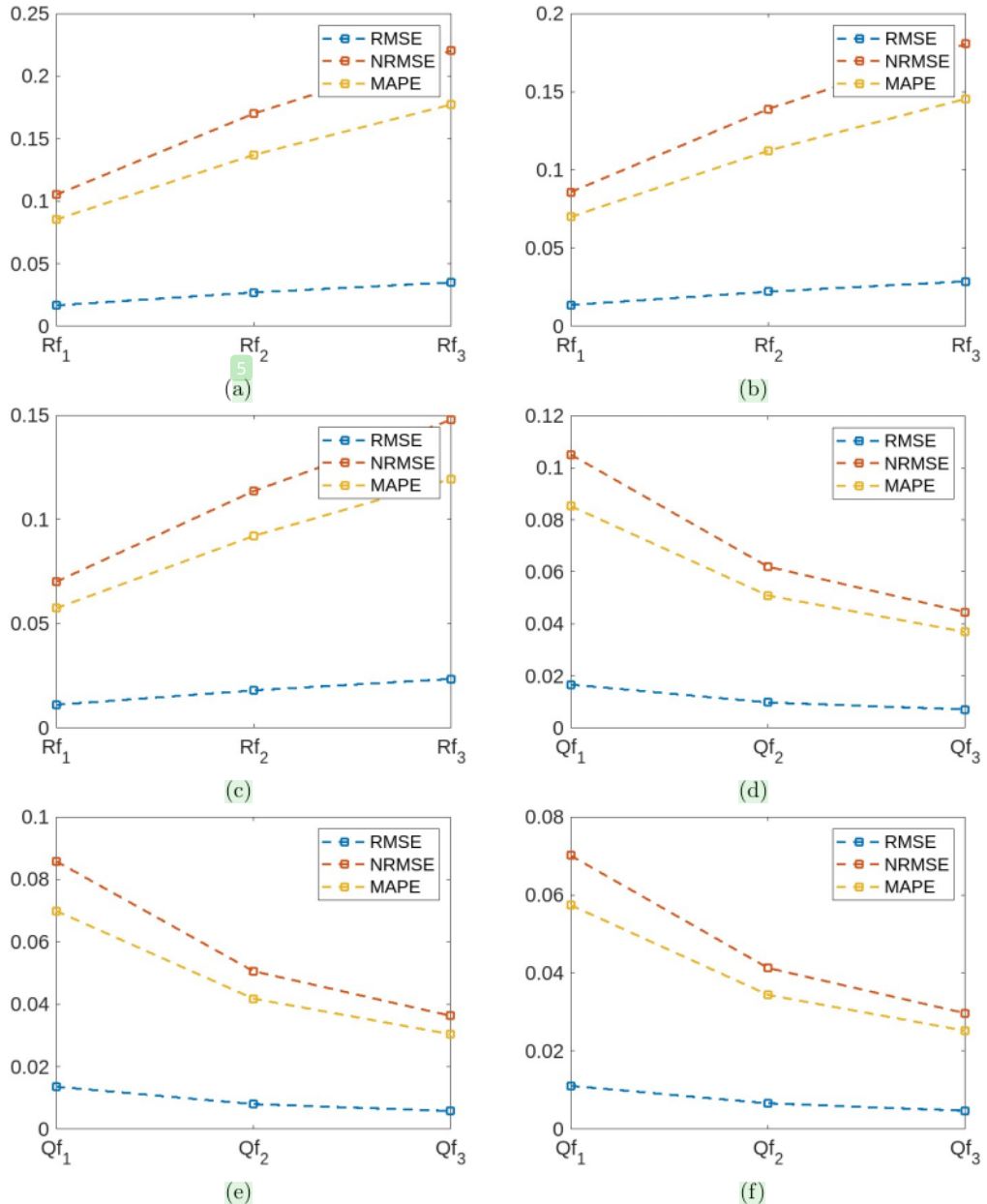


Figure 15: Profiles of RMSE, NRMSE and MAPE for varying R_f (15a, 15b, 15c) and Q_f (15d, 15e, 15f)

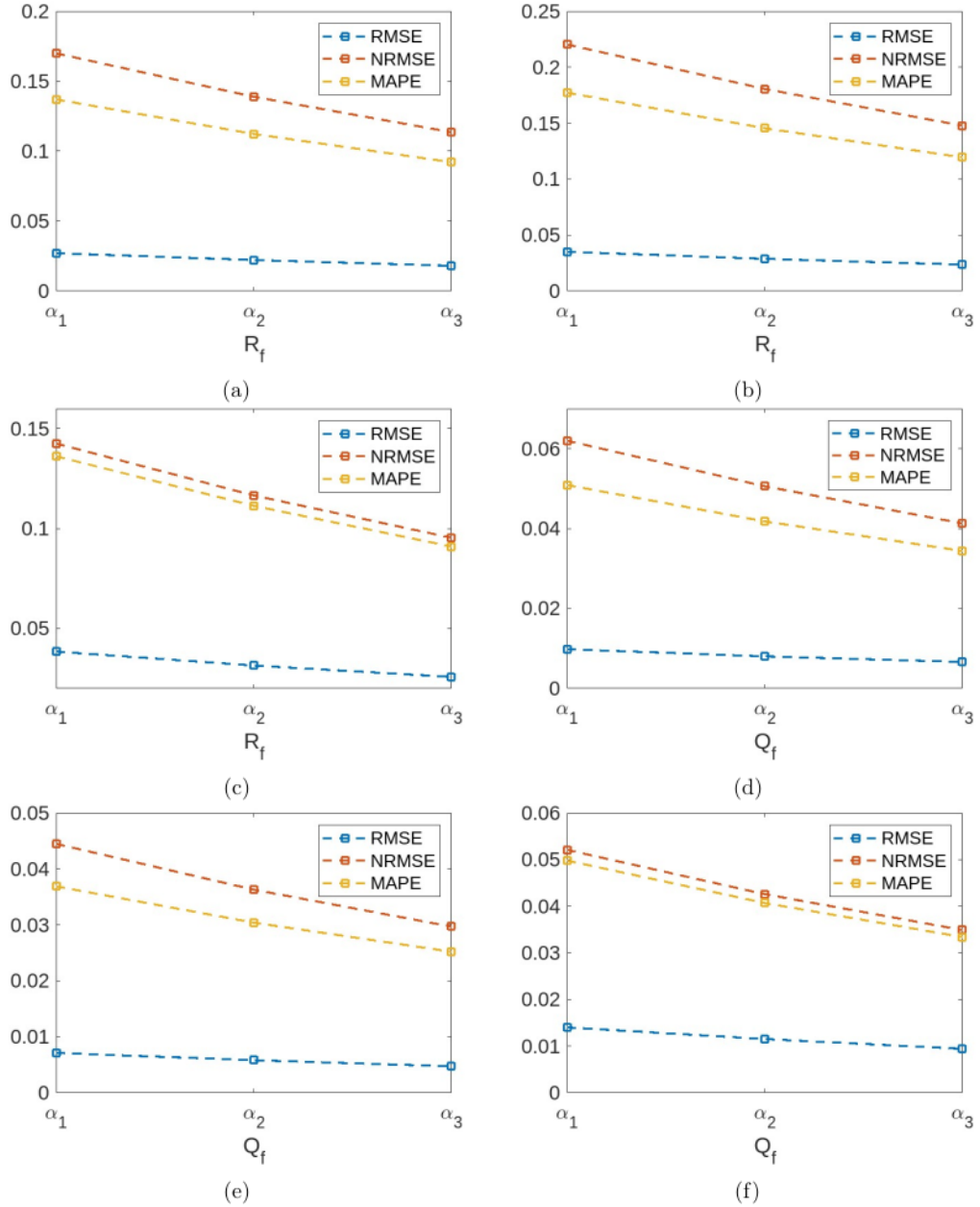


Figure 16: Profiles of *RMSE*, *NRMSE* and *MAPE* for varying fractional-order α of R_f (16a, 16b, 16c) and fractional-order α of Q_f (16d, 16e, 16f)

rate. As the results obtained, when the isolation rate increases, then infected number decreases, the susceptible number increases, the quarantined number decreases sharper and the recovered number decreases.

The highest sensitivity indices for each model parameter are achieved by the parameters of Λ ($\Gamma^{\mathcal{R}_0} = 1$), β ($\Gamma_{\beta}^{\mathcal{R}_0} = 1$) and δ ($\Gamma_{\delta}^{\mathcal{R}_0} = 1$) for the birth rate, infection and physical distancing rates respectively. This indicates that the birth, infection and physical distance rates provide the highest impact to increase the individuals infected by CoVid-19, if there are contact directly for two or more individuals. The smallest sensitivity index is only attained by ψ ($\Gamma_{\psi}^{\mathcal{R}_0} = -1$) for the natural mortality rate giving the impact of 100% to degrade the number of individuals infected by CoVid-19. Moreover, the infection β and physical distancing rates δ give the impact of 100% to increase the number of individuals infected by CoVid-19 because it is directly proportional to the basic reproduction number (\mathcal{R}_0). The similar values of sensitivity indices (44.10%) are attained by the isolation rate ϵ and recovery rate of infected individuals r , which mean that they have the same impact to degrade the infected number of CoVid-19.

At the disease-free ($\mathcal{R}_0 < 1$), the profiles of infected and quarantined numbers are more sloping than another one ($\mathcal{R}_0 > 1$). The susceptible number of $\mathcal{R}_0 < 1$ is higher than the susceptible number of $\mathcal{R}_0 > 1$ reflecting that the recovered number of $\mathcal{R}_0 < 1$ is lower than the recovered number of $\mathcal{R}_0 > 1$. The quarantined number of $\mathcal{R}_0 < 1$ approaches to zero because this is directly proportional to the infected number of $\mathcal{R}_0 < 1$ which also approaches to zero, i.e., the decreasing of infected number will affect the decreasing of quarantined number in this case.

Based on the values of *RMSE*, *NRMSE* and *MAPE* using FracEKF, the results are very meaningful for each fractional-order. Moreover, the higher fractional-order is the most accurate it is (accuracy value for $\alpha_3 = 0.8$) than two others (accuracy values for $\alpha_1 = 0.01$ and $\alpha_2 = 0.09$). The accuracy values for fractional-order $\alpha_3 = 0.8$ are given as follows:

$[RMSE; NRMSE; MAPE] = [5.2046e-04; 0.0033; 0.36\%]$ for phase \mathcal{T}_1 ,

$[RMSE; NRMSE; MAPE] = [0.0014; 0.0053; 0.26\%]$ for phase \mathcal{T}_2 ,

$[RMSE; NRMSE; MAPE] = [0.0027; 0.0101; 0.27\%]$ for phase \mathcal{T}_3 ,

$[RMSE; NRMSE; MAPE] = [0.0042; 0.0216; 0.27\%]$ for phase \mathcal{T}_4 .

Moreover, we obtain that the higher the varying Q_f is the smaller the error values are (it is closer to the report data for varying fractional-order α) and the higher the varying R_f is the higher the error values are (it gets further away from the report data for varying fractional-order α). The profiles *RMSE*, *NRMSE* and *MAPE* are mathematically stated as follows: $(Q_{f1}, Q_{f2}, Q_{f3}) \sim (\frac{1}{RMSE}, \frac{1}{NRMSE}, \frac{1}{MAPE})$, $(R_{f1}, R_{f2}, R_{f3}) \sim (RMSE, NRMSE, MAPE)$ and $(\alpha_1, \alpha_2, \alpha_3) \sim (\frac{1}{RMSE}, \frac{1}{NRMSE}, \frac{1}{MAPE})$, where Q_f is inversely proportional to *RMSE*, *NRMSE* and *MAPE*, R_f is directly proportional to *RMSE*, *NRMSE* and *MAPE* and α is inversely proportional to *RMSE*, *NRMSE* and *MAPE*.

10 Data availability

The report data of this study refers to the link below:

<https://siagacorona.semarangkota.go.id/halaman/covid19pertahun/2020>.

Use of AI tools declaration

The authors declare no use of AI tools in the creation of this paper.

Acknowledgements

The authors would like to thank the reviewers for their valuable comments and suggestions which helped to improve the paper. The first author received financial support for the research under contract number 121/UN3.1.17/PT/2022 by the Faculty of Advanced Technology and Multidiscipline, Universitas Airlangga, Indonesia.

References

- [1] Adnan et al., Investigation of time-fractional SIQR Covid-19 mathematical model with fractal-fractional Mittage-Leffler kernel, Alexandria Engineering Journal, vol. 61, no. 10, pp. 7771–7779, 2022, doi: 10.1016/j.aej.2022.01.030.
- [2] N. Ahmed, A. Raza, M. Rafiq, A. Ahmadian, N. Batool, and S. Salahshour, Numerical and bifurcation analysis of SIQR model, Chaos Solitons Fractals, vol. 150, p. 111133, 2021, doi: 10.1016/j.chaos.2021.111133.
- [3] M. N. Alenezi, F. S. Al-Anzi, and H. Alabdulrazzaq, Building a sensible SIR estimation model for COVID-19 outspread in Kuwait, Alexandria Engineering Journal, vol. 60, no. 3, pp. 3161–3175, 2021, doi: 10.1016/j.aej.2021.01.025.
- [4] Z. Ali, F. Rabiei, M. M. Rashidi, and T. Khodadadi, A fractional-order mathematical model for COVID-19 outbreak with the effect of symptomatic and asymptomatic transmissions, Eur Phys J Plus, vol. 137, no. 3, Mar. 2022, doi: 10.1140/epjp/s13360-022-02603-z.
- [5] R. T. Alqahtani, Mathematical model of SIR epidemic system (COVID-19) with fractional derivative: stability and numerical analysis, Adv Differ Equ, vol. 2021, no. 1, 2021, doi: 10.1186/s13662-020-03192-w.
- [6] F. S. Alshammari and M. A. Khan, Dynamic behaviors of a modified SIR model with nonlinear incidence and recovery rates, Alexandria Engineering Journal, vol. 60, no. 3, pp. 2997–3005, 2021, doi: 10.1016/j.aej.2021.01.023.
- [7] S. Annas, M. Isbar Pratama, M. Rifandi, W. Sanusi, and S. Side, Stability analysis and numerical simulation of SEIR model for pandemic COVID-19 spread in Indonesia, Chaos Solitons Fractals, vol. 139, p. 110072, 2020, doi: 10.1016/j.chaos.2020.110072.
- [8] M. R. K. Ariffin et al., Mathematical epidemiologic and simulation modelling of first wave COVID-19 in Malaysia, Sci Rep, vol. 11, no. 1, pp. 1–10, 2021, doi: 10.1038/s41598-021-99541-0.
- [9] S. Arshad, S. Khalid, S. Javed, N. Amin, and F. Nawaz, Modeling the impact of the vaccine on the COVID-19 epidemic transmission via fractional derivative, Eur Phys J Plus, vol. 137, no. 7, Jul. 2022, doi: 10.1140/epjp/s13360-022-02988-x.

- [10] A. Bani Younes, Z. Hasan, COVID-19: Modeling, prediction, and control, *Appl. Sci.* 10 (11), 2020, <https://doi.org/10.3390/app10113666>.
- [11] G. C. Calafiore, C. Novara, and C. Possieri, “A time-varying SIRD model for the COVID-19 contagion in Italy, *Annu Rev Control*, vol. 50, no. October, pp. 361–372, 2020, doi: 10.1016/j.arcontrol.2020.10.005.
- [12] Z. Cao, W. Feng, X. Wen, L. Zu, and M. Cheng, Dynamics of a stochastic SIQR epidemic model with standard incidence, *Physica A: Statistical Mechanics and its Applications*, vol. 527, pp. 1–12, 2019, doi: 10.1016/j.physa.2019.121180.
- [13] A. Cartocci, G. Cevenini, and P. Barbini, A compartment modeling approach to reconstruct and analyze gender and age-grouped CoViD-19 Italian data for decision-making strategies, *J Biomed Inform*, vol. 118, no. April, p. 103793, 2021, doi: 10.1016/j.jbi.2021.103793.
- [14] I. Cooper, A. Mondal, and C. G. Antonopoulos, A SIR Model Assumption for The Spread of COVID-19 in Different Communities, *Chaos Solitons Fractals*, vol. 139, no. January, p. 110057, 2020, doi: <https://doi.org/10.1016/j.chaos.2020.110057>.
- [15] N. Crokidakis, CoVid-19 spreading in Rio de Janeiro, Brazil: Do the policies of physical isolation really work?, *Chaos Solit. Fract.* 136, 109930, 2020, doi: <https://doi.org/10.1016/j.chaos.2020.109930>
- [16] N. Crokidakis, Modeling the early evolution of the CoVid-19 in Brazil; results from Susceptible-Infectious-Quarantined-Recovered (SIQR). *Int. J. Mod. Phys. C* 31, 1–8, 2020, doi: <https://doi.org/10.1142/S0129183120501351>
- [17] J. Demongeot, Q. Griette, and P. Magal, SI epidemic model applied to COVID-19 data in mainland China, *R Soc Open Sci*, vol. 7, no. 12, 2020, doi: 10.1098/rsos.201878.
- [18] O. Diekmann, J.A.P. Heesterbeek, J.A.J. Metz. On the definition and the computation of the basic reproduction ratio R_0 in models for infectious diseases in heterogeneous populations. *J Math Biol.* 1990;28:365–382. <https://doi.org/10.1007/BF00178324>.
- [19] P.S.R. Diniz, Kalman Filters. Adaptive Filtering: Algorithms and Practical Implementation, Springer International Publishing, Cham, pp. 431–456, 2020, <https://doi.org/10.1007/978-3-030-29057-314>.
- [20] R. Djalante et al., Review and analysis of current responses to COVID-19 in Indonesia: Period of January to March 2020, *Progress in Disaster Science*, vol. 6, 2020, doi: 10.1016/j.pdisas.2020.100091.
- [21] P. M. Fernandez, Z. Fernandez-Muniz, A. Cernea, J. Luis Fernandez-Martinez, and A. Kloczkowski, Comparison of three mathematical models for COVID-19 prediction, *Bioophys J*, vol. 122, no. 3S1, 2023, doi: 10.1016/j.bpj.2022.11.1616.
- [22] A. Fuady, N. Nuraini, and K. K. Sukandar, Targeted Vaccine Allocation Could Increase the COVID-19 Vaccine Benefits Amidst Its Lack of Availability: A Mathematical Modeling Study in Indonesia, *Vaccines (Basel)*, vol. 9, p. 462, 2021, doi: <https://doi.org/10.3390/vaccines9050462>.

- [23] K. M. Furati, I. O. Sarumi, and A. Q. M. Khaliq, Fractional model for the spread of COVID-19 subject to government intervention and public perception, *Appl Math Model*, vol. 95, pp. 89–105, Jul. 2021, doi: 10.1016/j.apm.2021.02.006.
- [24] M. Ghani, I. Q. Utami, F. W. Triyayuda, M. Afifah, A fractional SEIQR model on diphtheria disease. *Modeling Earth System and Environment*. 9, 2199–2219, 2023, <https://doi.org/10.1007/s40808-022-01615-z>.
- [25] A. Hasan, H. Susanto, V.R. Tjahjono, R. Kusdiantara, E.R.M. Putri, P. Hadisoemarto, N. Nuraini, A New Estimation Method for COVID-19 Time-Varying Reproduction Number Using Active Cases, *Scientific Reports*, 12, 6675, 2022, <https://doi.org/10.1038/s41598-022-10723-w>.
- [26] N.I. Hamdan, A. Kilicman, A fractional order SIR epidemic model for dengue transmission. *Chaos Solitons Fract* 114:55–62, 2018, <https://doi.org/10.1016/j.chaos.2018.06.031>.
- [27] N.I. Hamdan, A. Kilicman, Analysis of the fractional order dengue transmission model: a case study in Malaysia. *Adv Difer Equ* 114:3, 2019, <https://doi.org/10.1186/s13662-019-1981-z>.
- [28] S. He, Y. Peng, and K. Sun, SEIR modeling of the COVID-19 and its dynamics, *Nonlinear Dyn*, vol. 101, no. 3, pp. 1667–1680, 2020, doi: 10.1007/s11071-020-05743-y.
- [29] H. Khataee, I. Scheuring, A. Czirok, Z. Neufeld, Effects of physical distancing on the spreading of COVID-19 inferred from mobile phone data, *Sci. Rep.* 11 (1), 2021, <https://doi.org/10.1038/s41598-021-81308-2>.
- [30] N. A. Kudryashov, M. A. Chmykhov, and M. Vigdorowitsch, Analytical features of the SIR model and their applications to COVID-19, *Appl Math Model*, vol. 90, pp. 466–473, 2021, doi: 10.1016/j.apm.2020.08.057.
- [31] S. Kumar, K.K. Singh, P. Dixit, M. Kumar Bajpai, Kalman filter based short term prediction model for COVID-19 spread, *Appl. Intell.* 51 (5), 2714–2726, 2020, <https://doi.org/10.20546/ijcmas.2020.907.320>.
- [32] Y. Lin, and C. Xu, C, Finite difference/spectral approximations for the time-fractional diffusion equation. *J. Comput. Phys.* 225(2), 1533–1552, 2007 <https://doi.org/10.1016/j.jcp.2007.02.001>.
- [33] E. Mahase, Covid-19: What do we know about XBB.1.5 and should we be worried?, *BMJ*, vol. 380, no. May, p. p153, 2023, doi: 10.1136/bmj.p153.
- [34] T. T. Marinov and R. S. Marinova, Adaptive SIR model with vaccination: simultaneous identification of rates and functions illustrated with COVID-19, *Sci Rep*, pp. 1–13, 2022, doi: 10.1038/s41598-022-20276-7.
- [35] V. Martínez, A modified SIRD model to study the evolution of the covid-19 pandemic in spain, *Symmetry (Basel)*, vol. 13, no. 4, 2021, doi: 10.3390/sym13040723.

- [36] M. A. Nanda et al., The susceptible-infected-recovered-dead model for long-term identification of key epidemiological parameters of COVID-19 in Indonesia, International Journal of Electrical and Computer Engineering, vol. 12, no. 3, pp. 2900–2910, 2022, doi: 10.11591/ijece.v12i3.pp2900-2910.
- [37] T. Odagaki, Analysis of the outbreak of COVID-19 in Japan by SIQR model, Infect Dis Model, vol. 5, no. May 1982, pp. 691–698, 2020, doi: 10.1016/j.idm.2020.08.013.
- [38] H. A. Parhusip, S. Trihandaru, B. A. A. Wicaksono, D. Indrajaya, Y. Sardjono, and O. P. Vyas, Susceptible Vaccine Infected Removed (SVIR) Model for COVID-19 Cases in Indonesia, Science and Technology Indonesia, vol. 7, no. 3, pp. 400–408, 2022, doi: 10.26554/sti.2022.7.3.400-408.
- [39] I. Podlubny, Fractional Differential Equations: An Introduction to Fractional Derivatives, Fractional Differential Equations, to Methods of Their Solution and Some of Their Applications. Academic Press: California CA, USA. 1999.
- [40] R. Sameni, Mathematical Modeling of Epidemic Diseases; a Case Study of the COVID-19 Coronavirus, 2020 arXiv preprint arXiv:2003.11371, <https://doi.org/10.48550/arXiv.2003.11371>.
- [41] G. Sepulveda, A. J. Arenas, and G. González-Parra, Mathematical Modeling of COVID-19 Dynamics under Two Vaccination Doses and Delay Effects, Mathematics, vol. 11, no. 2, pp. 1–30, 2023, doi: 10.3390/math11020369.
- [42] J. Song, H. Xie, B. Gao, Y. Zhong, C. Gu, K.S. Choi, Maximum likelihood-based extended Kalman filter for COVID-19 prediction, Chaos, Solit. Fractals 146, 110922, 2021, <https://doi.org/10.1016/j.chaos.2021.110922>.
- [43] R. ud Din and E. A. Algehyne, Mathematical analysis of COVID-19 by using SIR model with convex incidence rate, Results Phys, vol. 23, no. October 2020, pp. 1–6, 2021, doi: 10.1016/j.rinp.2021.103970.
- [44] J. Yangla et al., Fractional dynamics of a Chikungunya transmission model, Sci Afr, vol. 21, Sep. 2023, doi: 10.1016/j.sciaf.2023.e01812.
- [45] R. Zhang and Y. Liu, A new Barbalat's lemma and Lyapunov stability theorem for fractional order systems, 29th Chinese control and decision conference (CCDC), IEEE, 3676–3681, 2017, doi: <http://dx.doi.org/10.1109/CCDC.2017.7979143>
- [46] X. Zhu, B. Gao, Y. Zhong, C. Gu, K.S. Choi, Extended Kalman filter for online soft tissue characterization based on Hunt-Crossley contact model, J. Mech. Behav. Biomed. Mater. 123, 104667, 2021 <https://doi.org/10.1016/j.jmbbm.2021.104667>.

FracEKF SIQR Model Analysis TURNITIN (Newest)

ORIGINALITY REPORT



PRIMARY SOURCES

1	www.mdpi.com Internet Source	1 %
2	Mohammad Ghani, Ika Qutsiati Utami, Fadillah Willis Triyayuda, Mutiara Afifah. "A fractional SEIQR model on diphtheria disease", <i>Modeling Earth Systems and Environment</i> , 2022 Publication	<1 %
3	dokumen.pub Internet Source	<1 %
4	www.aimspress.com Internet Source	<1 %
5	www.hindawi.com Internet Source	<1 %
6	scholar.unair.ac.id Internet Source	<1 %
7	journals.itb.ac.id Internet Source	<1 %
8	123dok.org Internet Source	<1 %

<1 %

9

www.medrxiv.org

Internet Source

<1 %

10

Mohammad Ghani, Indah Fahmiyah, Ratih Ardiati Ningrum, Ananta Adhi Wardana.

"Dynamical analysis of spatio-temporal CoVid-19 model", International Journal of Dynamics and Control, 2024

Publication

<1 %

11

journals.semnan.ac.ir

Internet Source

<1 %

12

pubmed.ncbi.nlm.nih.gov

Internet Source

<1 %

13

"Mathematical Analysis for Transmission of COVID-19", Springer Science and Business Media LLC, 2021

Publication

<1 %

14

Mohammad Ghani. "Dynamics of spatio-temporal HIV–AIDS model with the treatments of HAART and immunotherapy", International Journal of Dynamics and Control, 2023

Publication

<1 %

15

Zhongwei Cao, Wei Feng, Xiangdan Wen, Li Zu, Ming Cheng. "Dynamics of a stochastic

<1 %

SIQR epidemic model with standard incidence", Physica A: Statistical Mechanics and its Applications, 2019

Publication

- | | | |
|----|--|------|
| 16 | hal.archives-ouvertes.fr | <1 % |
| 17 | scik.org | <1 % |
| 18 | www.pccouncil.org | <1 % |
| 19 | Mohammad Ghani, Yolanda Norasia, Wahyuni Ningsih. "Dynamics of CoVid-19 Disease in Semarang, Indonesia: Stability, Optimal Control, and Model-Fitting", Differential Equations and Dynamical Systems, 2023 | <1 % |
| 20 | ojs3.unpatti.ac.id | <1 % |
| 21 | b-ok.cc | <1 % |
| 22 | mdpi-res.com | <1 % |
| 23 | Jialu Song, Hujin Xie, Bingbing Gao, Yongmin Zhong, Chengfan Gu, Kup-Sze Choi. "Maximum likelihood-based extended Kalman | <1 % |

filter for COVID-19 prediction", Chaos,
Solitons & Fractals, 2021

Publication

- 24 Submitted to University College London **<1 %**
Student Paper
-
- 25 Zhen, Xiaoxing. "Incorporating Drought and Marker Associated Traits into the DSSAT Model", Auburn University, 2022 **<1 %**
Publication
-
- 26 Zhenhua Yu, Jingmeng Zhang, Yun Zhang, Xuya Cong, Xiaobo Li, Almetwally M. Mostafa. "Mathematical modeling and simulation for COVID-19 with mutant and quarantined strategy", Chaos, Solitons & Fractals, 2024 **<1 %**
Publication
-
- 27 coek.info **<1 %**
Internet Source
-
- 28 inst.eecs.berkeley.edu **<1 %**
Internet Source
-
- 29 www.frontiersin.org **<1 %**
Internet Source
-
- 30 www.ncbi.nlm.nih.gov **<1 %**
Internet Source
-
- 31 www.techscience.com **<1 %**
Internet Source
-

- 32 Guo, H.. "Crank-Nicolson least-squares Galerkin procedures for parabolic integro-differential equations", Applied Mathematics and Computation, 20060915 <1 %
Publication
-
- 33 Submitted to Universitas Airlangga <1 %
Student Paper
-
- 34 "Numerical Analysis and Its Applications", Springer Science and Business Media LLC, 2013 <1 %
Publication
-
- 35 Anip Kumar Paul, Neerob Basak, Md Abdul Kuddus. "A mathematical model for simulating the transmission dynamics of COVID-19 using the Caputo–Fabrizio fractional-order derivative with nonsingular kernel", Informatics in Medicine Unlocked, 2023 <1 %
Publication
-
- 36 Mark C. Kerstetter. "A KWIC permuted list of articles in the SIGCSE Bulletin 1983", ACM SIGCSE Bulletin, 9/1/1984 <1 %
Publication
-
- 37 Muhammad Achirul Nanda, Anifatul Faricha, Siti Maghfirotul Ulyah, Ni'matut Tamimah et al. "The susceptible-infected-recovered-dead model for long-term identification of key <1 %

epidemiological parameters of COVID-19 in Indonesia", International Journal of Electrical and Computer Engineering (IJECE), 2022

Publication

- 38 Reza Shahabifar, Mahboubeh Molavi-Arbshahi, Omid Nikan. "Numerical analysis of COVID-19 model with Caputo fractional order derivative", AIP Advances, 2024 <1 %
Publication
- 39 Submitted to Universiti Teknologi MARA <1 %
Student Paper
- 40 ejde.math.txstate.edu <1 %
Internet Source
- 41 Voigt, Matthias, Visvanathan Ramesh, Jonnalagadda Vinay, and Dennis LeMieux. "", Thermosense XXIX, 2007. <1 %
Publication
- 42 "Time Delay Systems", Springer Science and Business Media LLC, 2017 <1 %
Publication
- 43 Shu Tang Liu, Yong Ping Zhang, Chang An Liu. "Fractal Control and Its Applications", Springer Science and Business Media LLC, 2020 <1 %
Publication
- 44 Submitted to University of New South Wales <1 %
Student Paper

- 45 Zakaria Yaagoub, Karam Allali. "Global Stability of Multi-Strain SEIR Epidemic Model with Vaccination Strategy", Mathematical and Computational Applications, 2023
Publication <1 %
- 46 Zizhen Zhang, Ghaus ur Rahman, Kottakkaran Sooppy Nisar, Ravi Agarwal. "Incorporating convex incidence rate and public awareness program in modelling drinking abuse and novel control", Physica Scripta, 2021
Publication <1 %
- 47 Submitted to Chester College of Higher Education <1 %
Student Paper
- 48 Adnan, Amir Ali, Mati ur Rahman, Muhammad Arfan, Zahir Shah, Poom Kumam, Wejdan Deebani. "Investigation of time-fractional SIQR Covid-19 mathematical model with fractal-fractional Mittage-Leffler kernel", Alexandria Engineering Journal, 2022
Publication <1 %
- 49 Lislaine Cristina Cardoso, Rubens Figueiredo Camargo, Fernando Luiz Pio dos Santos, José Paulo Carvalho Dos Santos. "Global stability analysis of a fractional differential system in hepatitis B", Chaos, Solitons & Fractals, 2021
Publication <1 %

- 50 Ozlem Defterli. "Comparative analysis of fractional order dengue model with temperature effect via singular and non-singular operators", Chaos, Solitons & Fractals, 2021 <1 %
Publication
-
- 51 Pitchaimani M, Brasanna Devi M. "Stochastic dynamical probes in a triple delayed SICR model with general incidence rate and immunization strategies", Chaos, Solitons & Fractals, 2021 <1 %
Publication
-
- 52 Takashi Odagaki. "Analysis of the outbreak of COVID-19 in Japan by SIQR model", Infectious Disease Modelling, 2020 <1 %
Publication
-
- 53 Zenebe Shiferaw Kifle, Legesse Lemecha Obsu. "Mathematical modeling for COVID-19 transmission dynamics: A case study in Ethiopia", Results in Physics, 2022 <1 %
Publication
-
- 54 earsiv.cankaya.edu.tr:8080 <1 %
Internet Source
-
- 55 magazine.mdpu.org.ua <1 %
Internet Source
-
- 56 rcin.org.pl <1 %
Internet Source

- 57 Luisa Ferrari, Giuseppe Gerardi, Giancarlo Manzi, Alessandra Micheletti, Federica Nicolussi, Elia Biganzoli, Silvia Salini. "Modeling Provincial Covid-19 Epidemic Data Using an Adjusted Time-Dependent SIRD Model", International Journal of Environmental Research and Public Health, 2021
Publication
-
- 58 Xinhe Zhu, Bingbing Gao, Yongmin Zhong, Chengfan Gu, Kup-Sze Choi. "Extended Kalman filter based on stochastic epidemiological model for COVID-19 modelling", Computers in Biology and Medicine, 2021
Publication
-
- 59 Agus Hasan, Endah Putri, Hadi Susanto, Nuning Nuraini. "Data-driven modeling and forecasting of COVID-19 outbreak for public policy making", Cold Spring Harbor Laboratory, 2020
Publication
-
- 60 Cristiane M. Batistela, Diego P.F. Correa, Átila M. Bueno, José Roberto Castilho Piqueira. "SIRSi-vaccine dynamical model for the Covid-19 pandemic", ISA Transactions, 2023
Publication
-

- 61 H X Shen, X Li, L Chen, H H Xun, W X Chen. "Estimation of state of charge of lithium battery based on parameter identification of fractional order model", Journal of Physics: Conference Series, 2021 <1 %
Publication
-
- 62 Hasib Khan, Farooq Ahmad, Osman Tunç, Muhammad Idrees. "On fractal-fractional Covid-19 mathematical model", Chaos, Solitons & Fractals, 2022 <1 %
Publication
-
- 63 Naba Kumar Goswami, Samson Olaniyi, Sulaimon F. Abimbade, Furaha M. Chuma. "A mathematical model for investigating the effect of media awareness programs on the spread of COVID-19 with optimal control", Healthcare Analytics, 2024 <1 %
Publication
-
- 64 Robert Prem Kumar, Sanjoy Basu, Dipankar Ghosh, Pasanta Kumar Santra, G. S. Mahapatra. "Dynamical analysis of novel -19 epidemic model with non-monotonic incidence function", Journal of Public Affairs, 2021 <1 %
Publication
-
- 65 Shah Hussain, Elissa Nadia Madi, Hasib Khan, Haseena Gulzar, Sina Etemad, Shahram Rezapour, Mohammed K. A. Kaabar. "On the <1 %

Stochastic Modeling of COVID-19 under the Environmental White Noise", Journal of Function Spaces, 2022

Publication

-
- 66 Shyamsunder, S. Bhatter, K. Jangid, A. Abidemi, K.M. Owolabi, S.D. Purohit. "A new fractional mathematical model to study the impact of vaccination on COVID-19 outbreaks", Decision Analytics Journal, 2023 <1 %
- Publication
-
- 67 Sk Shahid Nadim, Indrajit Ghosh, Joydev Chattopadhyay. "Short-term predictions and prevention strategies for COVID-19: A model-based study", Applied Mathematics and Computation, 2021 <1 %
- Publication
-
- 68 Tanatorn Intarapanya, Apichat Suratanee, Sittiporn Pattaradilokrat, Kitiporn Plaimas. "Modeling the Spread of COVID-19 with the Control of Mixed Vaccine Types during the Pandemic in Thailand", Tropical Medicine and Infectious Disease, 2023 <1 %
- Publication
-
- 69 Zubair Ahmad, Sherif A. El-Kafrawy, Thamir A. Alandijany, Francesco Giannino et al. "A Global Report on the Dynamics of COVID-19 with Quarantine and Hospitalization: A Fractional <1 %

Order Model with Non-Local Kernel",
Computational Biology and Chemistry, 2022

Publication

70 advancesindifferenceequations.springeropen.com <1 %
Internet Source

71 dergipark.org.tr <1 %
Internet Source

72 ejurnal.ung.ac.id <1 %
Internet Source

73 journals.atu.ac.ir <1 %
Internet Source

74 journals.plos.org <1 %
Internet Source

75 jurnalsaintek.uinsby.ac.id <1 %
Internet Source

76 link.springer.com <1 %
Internet Source

77 van den Driessche, P.. "Modeling relapse in
infectious diseases", Mathematical
Biosciences, 200705 <1 %
Publication

78 webs-deim.urv.cat <1 %
Internet Source

79 www.arxiv-vanity.com <1 %
Internet Source

- 80 www.freepatentsonline.com <1 %
Internet Source
- 81 www.int-arch-photogramm-remote-sens-spatial-inf-sci.net <1 %
Internet Source
- 82 www.researchgate.net <1 %
Internet Source
- 83 Hadi Jahanshahi, Jesus M. Munoz-Pacheco, Stelios Bekiros, Naif D. Alotaibi. "A fractional-order SIRD model with time-dependent memory indexes for encompassing the multi-fractional characteristics of the COVID-19", Chaos, Solitons & Fractals, 2021 <1 %
Publication
- 84 Scherer, R.. "Numerical treatment of fractional heat equations", Applied Numerical Mathematics, 200808 <1 %
Publication
- 85 Sharmin Sultana, Gilberto González-Parra, Abraham J. Arenas. "Mathematical Modeling of Toxoplasmosis in Cats with Two Time Delays under Environmental Effects", Mathematics, 2023 <1 %
Publication
- 86 Suwardi Annas, Muh. Isbar Pratama, Muh. Rifandi, Wahidah Sanusi, Syafruddin Side. "Stability Analysis and Numerical Simulation <1 %

of SEIR Model for pandemic COVID-19 spread in Indonesia", *Chaos, Solitons & Fractals*, 2020

Publication

- 87 Ugo Avila-Ponce de León, Ángel G.C. Pérez, Eric Avila-Vales. "An SEIARD epidemic model for COVID-19 in Mexico: Mathematical analysis and state-level forecast", *Chaos, Solitons & Fractals*, 2020 <1 %
- Publication
-
- 88 Karl Peter Hadeler. "Topics in Mathematical Biology", Springer Science and Business Media LLC, 2017 <1 %
- Publication
-
- 89 LONGXING QI, JING-AN CUI, YUAN GAO, HUAIPING ZHU. "MODELING THE SCHISTOSOMIASIS ON THE ISLETS IN NANJING", *International Journal of Biomathematics*, 2012 <1 %
- Publication
-
- 90 Shiferaw Geremew Kebede, Assia Guezane Lakoud. "Analysis of mathematical model involving nonlinear systems of Caputo–Fabrizio fractional differential equation", *Boundary Value Problems*, 2023 <1 %
- Publication
-
- 91 TAO-QIAN TANG, RASHID JAN, ZAID KHAN, ZAHIR SHAH, NARCISA VRINCEANU, MIHAELA RACHERIU. "MODELING THE <1 %

DYNAMICS OF CHRONIC MYELOGENOUS LEUKEMIA THROUGH FRACTIONAL-CALCULUS", Fractals, 2022

Publication

Exclude quotes On

Exclude bibliography On

Exclude matches Off